Design and Analysis of 60kW dc-dc converter for Hybrid Electric Vehicles

A dissertation submitted in partial fulfillment of the requirement for the award of degree of

Master of Engineering

in

POWER SYSTEMS AND ELECTRIC DRIVES

Submitted by

Dharam Dutta

Roll No. 801141011

Under the supervision of

Mr. Souvik Ganguli

Assistant Professor, EIED

Thapar University, Patiala

Electrical and Instrumentation Engineering Department

Thapar University, Patiala – 147004

DECLARATION

I hereby declare that the work which is being presented in the dissertation entitled, **"Design and Analysis of 60kW dc-dc converter for Hybrid Electric Vehicles"** in partial fulfilment of the requirement for the award of degree of Master of Engineering in Power System and Electric Drive submitted in Electrical and Instrumentation Engineering Department of Thapar University, Patiala, is an authentic record of my own work carried out under the supervision of Mr.Souvik Ganguli, Assistant Professor, EIED and refers other researcher's work which are duly listed in the reference section.

The matter presented in this dissertation has not been submitted in any other University/Institute for the award of degree.

Date: 12/7/13

Dharam Dutta

Dharam Dutta

Roll No: 801141011

It is certified that the above statement made by the student is correct to the best of my knowledge and belief.

Ganguli 12/07/13

Mr.Souvik Ganguli

Assistant Professor

EIED, Thapar University

Countersigned by:

S. Ghosh

Head

EIED, Thapar University

Patiala-147004

Dean of Academic Affairs

Thapar University

Patiala- 147004

ACKNOWLEDGEMENT

First of all, I would like to express my gratitude to **Mr.Souvik Ganguli, Assistant Professor**, Electrical and Instrumentation Engineering Department, Thapar University, Patiala for his patient guidance and support throughout my work. I am truly very fortunate to have the opportunity to work with him. I found his guidance to be extremely valuable.

I am also thankful to **Professor Dr.Smarajit Ghosh, Head of the Department**, Electrical and Instrumentation Engineering Department and **Ms.Manbir Kaur, Associate Professor and PG coordinator** for their invaluable suggestions and constant encouragement all through the work. I would also like to convey my sincerest gratitude and indebtedness to entire faculty and staff of Electrical and Instrumentation Engineering Department. I would also like to thank my friends who devoted their valuable time and helped me in all possible ways towards successful completion of this work. I thank all those who have contributed directly or indirectly to this work.

Lastly, I would like to thank my parents for their unconditional support and encouragement.

Dharam Dutta

Roll no. 801141011

ABSTRACT

This work aims at the design and analysis of Bidirectional dc-dc converter with two different core materials and different core shape at 20 kHz 450 V voltage level. The losses and efficiency of converters are studied at a specified frequency and voltage. Converter designed is analysed at 450 voltage level. Results show that losses are higher in EC-70 core at 20 kHz, 450V system. The result suggests that the use of iron powder as core material increases the losses of the converter. The result also shows that the core shape ETD-49 has smaller core losses as compared with the EC-70 core. Designed converter is then analysed by developing state space averaging model taking into consideration designed values of resistance and reactance of the components of the bidirectional converter. Finally approximate state space model then analysed with bode plots and pole location and stability of the transfer functions are being checked.

LIST OF SYMBOLS

K	Duty Ratio of Switches
$D_{1,2}$	Diode
R	Resistor
L	Inductor of Converter
I_L	Inductor Current
U_{IN}	Input voltage of the converter
U_O	Output voltage of the converter
f_{sw}	Switching frequency of converter (Hz)
t_{ON}	Switch on time (s)
t_{OFF}	Switch off time (s)
T_{sw}	Switching Time Period ($1/ f_{SW}$)
S	Switch
I_{IN}	Converter Input Current
I_{LOAD}	Converter Load Current
HEV	Hybrid Electrical Vehicle
P_O	Output Power

TABLE OF CONTENTS

LIST OF FIGURES

CHAPTER 1

INTRODUCTION

1.1 BACKGROUND OF WORK

The world witnessed the new path when the first modern hybrid electric car was sold in Japan. After about two years, United States sold its Honda insight. These two followed by Honda civic, marked a tremendous change in the type of cars being offered to common man: Vehicles that bring some values of the battery electric vehicles into the conventional gasoline powered truck that we have been using for many years. Hybrid vehicle though are not as clean as hydrogen fuel cell vehicles, offers less emission than today's conventional vehicles and high fuel economy, thus their led a stepping stone to zero emission vehicles.

1.2 NEED FOR HYBRID ELECTRIC VEHICLES

The primary importance of hybrid technology for cars and trucks is its potential to increase fuel economy drastically while meeting today's most stringent tailpipe emission standards (excluding the zero emission vehicle standard). At the same time, the performance of hybrid vehicles can equal or even surpass that of most conventional vehicles. Moreover, hybrids can play a critical role in helping to bring the technology of motors, power electronics, and batteries to maturity and in reducing their cost. Such changes are vital to the success of future hydrogen fuel cell and other zero emission vehicles. Thus hybrids could be the key element to address our growing insecurity and environmental problems. Whether hybrids live up to their potential hinges on automakers and governments embracing them as one means of moving toward a secure energy future and a healthier environment.

1.3 THE GLOBAL VEHICLES EMISSION CHALLENGES

With the rise in global warming and doubling of CO_2 emissions from vehicles in the environment, the importance of addressing fuel efficiency in road transport is rising on global and national environment, energy, and climate change agendas. Road transport is responsible for 17-18% of global CO_2 emissions from fossil fuel combustion and in most countries transport CO_2 emissions are growing at a much faster rate than total CO_2 emissions. Road transport growth projection and car ownership for the next few decades show that road transport will have dominance, despite the rapid growth in shipping and aviation.

Significant fuel economy improvements in road transport are required to stabilize and eventually decrease greenhouse gas emissions from the transport sector; past improvements in efficiency will not be adequate to compensate for the steady increase in traffic volume. The United Nations Intergovernmental Panel on Climate Change (IPCC) states that an ambitious 50-80% reduction in global CO_2 emissions is required by 2050 (as compared to 2000 levels) in order to limit temperature rise to 2-2.4 degrees Celsius and stabilize atmospheric CO_2 concentration at 450 parts per million (ppm), thus avoiding severe climate change. Doubling the fuel efficiency of road vehicles (in particular light duty cars, vans and trucks) is one of the most cost-effective and accessible measures towards achieving global stabilization of CO_2 emissions.

However, the targets for both global CO_2 emission reduction and fuel efficiency improvement require that all countries adopt cleaner technology on a large scale. Conventional vehicles with internal combustion engines (ICE) provide good performance and long operating range by utilizing the high energy-density advantages of petroleum fuels. However, conventional ICE vehicles bear the disadvantages of poor fuel economy as well as environmental pollution. The main reasons for their poor fuel economy are as follows (1)engine fuel efficiency characteristics are mismatched with the real operation requirements (2) dissipation of vehicle kinetic energy during braking, especially while operating in urban areas, and (3) low efficiency of hydraulic transmission in current automobiles in stop-and-go driving patterns.

Battery-powered Electric Vehicles (EV), on the other hand, possess some advantages over conventional Internal Combustion Engines (ICE) vehicles, such as high energy

efficiency and zero environmental pollution. However, the performance, especially the operation range per battery charge, is far less competitive than ICE vehicles, due to the lower energy content of the batteries in comparison to the energy content of gasoline. Hybrid electric vehicles (HEV), which use two power sources — a primary power source and a secondary power source — have the advantages of both ICE vehicles and EV and overcome their disadvantages .Typical power electronic circuits used in hybrid electric vehicles (HEV) include inverters and DC-DC converters. In some electrical vehicles the high voltage battery is connected directly to the inverters; however an alternate is to have a dc-dc converter in between to maintain a fixed dc voltage for the inverter. In this thesis we provide topology, design and analysis of this DC-DC converter for hybrid electrical vehicle applications (HEV).

A critical factor propelling the shift from conventional gasoline/diesel engine vehicles to electric hybrid and fuel cell vehicles is the improvement in performance, size and cost of power electronics circuits over the past decade, with parallel improvements in sensors and microprocessors. Among the types of power electronics circuits used in a HEV, we use the configuration of a typical series HEV powertrain as shown in Fig 1.1. In this configuration, the internal combustion engine (ICE) drives a three-phase permanent magnet synchronous generator, whose output is a three-phase voltage with variable frequency and variable voltage. This output needs to be rectified to a direct current (DC) voltage. The front wheels are driven by an induction motor which needs to be controlled by a voltage source inverter (VSI) or a current source inverter (CSI). An energy storage system is connected to the DC bus, between the generator/rectifier output and the inverter. However, there is a bidirectional DC–DC converter that manages the charge/discharge of the battery, as well as controlling the DC bus voltage.

In addition, auxiliary components, such as headlights, wipers, entertainment systems, heat seats, and so on, run from the 14V auxiliary battery. Most advanced hybrid vehicles no longer have an alternator, which means the 14V battery needs to be charged from the high-voltage (HV) battery. On the other hand, even if an alternator is present, when the engine is off, the 14V battery can still be drained quickly without proper charge maintenance [2]. Therefore, it is necessary to have a DC–DC converter to charge the 14V battery from the

hybrid battery. For Plug-in Hybrid Electric Vehicles (PHEV), there is also a battery charger installed on the vehicle or in the charging station.

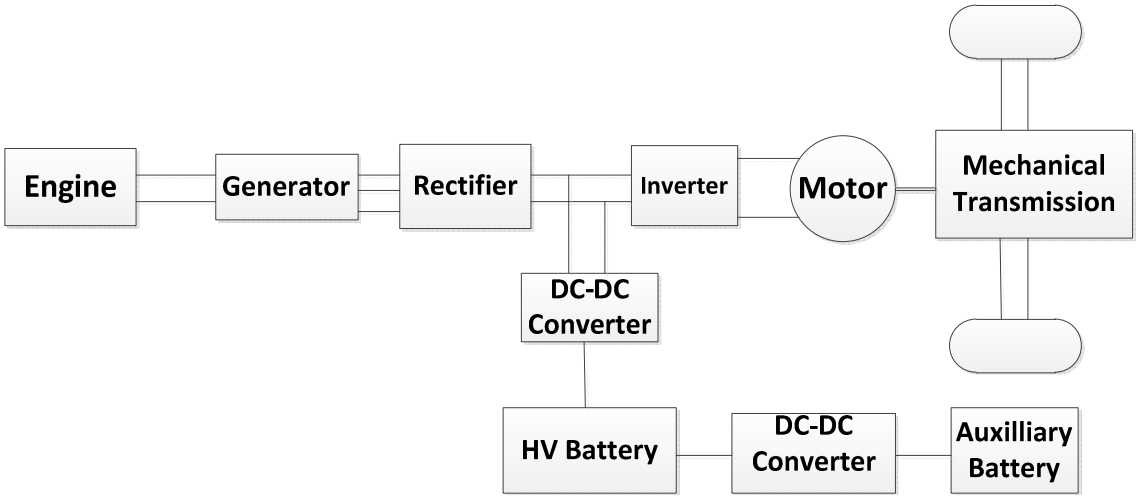

Fig. 1.1 Power electronic converters used in HEV [1].

1.4 PURPOSE OF WORK

One of the most critical issues for the environment today is pollution generated by hydrocarbon combustion, which is one of the main sources of power for transportation. Hybrid Electric Vehicles (HEV) and Electric Vehicles (EV) are rapidly advancing as an alternative power trains for green transportation. The vehicles' electrification not only involves the traction parts, but it is also generating new applications for electric power conversion. One of the key blocks inside hybrid electric vehicles is the DC–DC converter for auxiliary power supply of electric loads. This converter has to be capable of handling the energy transfer from the high voltage DC bus to the battery and vice versa (used for electric traction).

The purpose of this work is to design a 60 kW DC-DC converter for hybrid electric vehicle applications. The converter is able to maintain a constant DC link voltage when it is in motoring (or Up) mode of operation and energy flows from the DC voltage link bus to the battery when it works in generating (Down) mode of operation. The aim is to study the operation of the DC-DC converter at 20 kHz and different core materials with two different

shapes for the inductor. The objective is to analyse losses and the efficiency at 60 kW followed by analysis of the designed converter using state space averaging technique.

1.5 ORGANIZATION OF THE DISSERTATION

This dissertation is organized as follows

Chapter 2 contains the literature review of papers related to the work. It contains the literature review of papers used in the designing and analysis of dc-dc converter.

Chapter 3 focuses on the overview of Hybrid vehicle working and the circuit deducing the operation of bidirectional converter. It also focuses on the total loss calculation followed by design of the inductors and the capacitors.

Chapter 4 discusses the case study of the power converter being designed. It shows the total losses and the respective efficiency of the designed converters.

Chapter 5 discusses on the analysis of the designed converter as per the given parameters. It gives insight of state space averaging technique followed by their frequency domain analysis.

Chapter 6 contains conclusion and future scope of the work.

CHAPTER 2

LITERATURE REVIEW

2.1 INTRODUCTION

Electric vehicles (EV) and Hybrid Electric Vehicles (HEV) have gained much attention, especially in the context of growing concerns about global warming and aspects of the energy security associated with road transport. In this chapter, review of the literature is done which provides a deep insight of the technology aspects of power converter designing and its state space modelling for bidirectional operation with the current state of the research and development in the field.

2.2 LITERATURE REVIEW

Peng *et al.* [2] gave an overview of the topologies, design, and thermal management, and control of power electronics circuits in hybrid vehicle applications. Power electronics circuits played a significant role in the success of electric, hybrid and fuel cell vehicles. Conventional circuit topologies viz. buck converters, voltage source inverters and bidirectional boost converters are compared on the basis of system cost, efficiency, controllability, thermal management, voltage and current capability, and packaging issues. This paper presented an overview of the power electronics circuits for HEV applications focusing on circuit topologies, analysis and thermal management. Novel power switching devices and power electronics systems have the potential to improve the overall performance of hybrid vehicles.

Rim *et al.* [3] presented the state space averaging of non linear boost followed by derivation of DC equivalent and small signal equivalent circuit models of non ideal boost converter.

Moussa *et al.* [4] presented the review of state space averaging method and method of PWM switch with the graphical result for comparison. Both methods simplified considerably the analysis of the non-linear converter system.

Mahdavi *et al.* [5] illustrated the point that the generalised state space model works well only within specific converter topologies and parametric limits where the topology number of components do not defines the model approximation order. Basic dc/dc single ended topologies were taken into consideration and then finally simulation results were compared to the exact topological state space model. Approximation order is an important factor in improving the model accuracy is concluded from the work in case when the switching frequency is not much higher than the converter natural frequencies.

Schupbachj *et al.* [6] presented an analysis, design, and comparative study of several bi-directional non-isolated DC-DC converter topologies that could be considered potential candidates for the power electronic interface of HEV energy power sources, in particular an ultra-capacitor pack.

Yalamanchili *et al.* [7] presented a review of multiple input dc-dc power electronic converters (MI-PEC) devoted to combine the power flow from several on-board energy sources of an EV/HV and several multi-input dc–dc converters based on various topologies were studied and analyzed.

Davoudi *et al.* [8] presented a new approach for generating the state space average value model for PWM converter in both continuous conduction mode and discontinuous conduction model. Duty ratio constraint and the correction terms were extracted numerically using the detailed simulation and were expressed as non linear functions of duty cycle. The functions of the duty-ratio constraint and correction term were obtained numerically by running the detailed simulation.

Jih-Sheng *et al.* [9] described the significance of energy management of power converters and their circuit topology options for efficiency, size and cost considerations. Whether isolated or non-isolated, soft switching techniques have been widely used in high-power bidirectional dc–dc converters. Through some design examples, the component selection and

circuit design optimization were discussed, and their efficiency evaluation results were also given.

Bellur *et al.* [10] presented an overview of state-of-the-art DC-DC converters used in Battery Electric Vehicles (BEVs), Hybrid Electric Vehicles (HEVs), and Fuel Cell Vehicles (FCVs). Several DC-DC converters such as isolated or non-isolated, half-bridge or full-bridge, unidirectional and bidirectional topologies, and their applications in electric vehicles were presented.

Silvestre *et al.* [11] described a bidirectional DC-DC converter for a small electric vehicle. The DC-DC converter designed and tested was capable of raising the voltage from the battery pack 96V(nominal) to 600V necessary to feed the Variable Frequency Drive(VFD) that controls the induction motor and was also capable of working in the opposite direction (600V to 96V) in order to capture energy from regenerative braking and downhill driving.

Nwosu [12] presented the state-space averaging of a non-ideal boost converter followed by derivation of DC state and small signal AC state modelling of the converter.

Du.Y *et al.* [13] compared and reviewed several non-isolated bidirectional converters suited for charge station applications. A charge station architecture for municipal parking decks had been proposed, which had a DC micro grid to interface with multiple DC-DC chargers, distributed renewable power generations and energy storage and provided functionalities of normal and rapid charging, grid support such as reactive and real power injection (including V2G), current harmonic filtering and load balance. Several non-isolated bidirectional DC-DC converters suited for charge station applications had been reviewed and compared, as the major focus to be studied by Half Bridge converter was a good candidate but it was difficult to maintain high efficiency in wide battery pack voltage range. Finally three-level bi-directional DC-DC converter was suggested to be employed in this application.

Ahmadi *et al.* [14] presented a new bidirectional converter employing Gallium Nitride (GaN) power transistors in which Zero-Voltage-Transition (ZVT) switching was provided for all switches to dramatically reduce the switching losses regardless of power flow direction. Bidirectional dc-dc converters are used in many applications when bidirectional energy

transfer between two DC buses is needed. They are used as an interface circuit between ultra-capacitor and DC bus in a Hybrid Electric Vehicle (HEV). Since the voltage levels of the ultra-capacitor and DC bus are different, the interface circuitry must be able to increase or decrease the voltage level in each power flow direction while limiting the current. The soft-switched GaN power transistors resulted in a significant increase in the efficiency of the new converter as compared to that of conventional hard-switched bidirectional converters.

Yang *et al.* [15] presented the dynamic characteristics of the bidirectional DC-DC converter using a current generator instead of load resistor .Transfer functions are derived by applying the state space averaging method. Transient response characteristics of the converter are confirmed when the direction of power flow changed.

Zahedi *et al.* [16] presented different modelling approaches for an isolated bidirectional dc-dc converter to be used in analysis and simulation of a hybrid electric ship. The models were verified by comparison with simulation results of detailed switching model in PLECS software and the advantages and disadvantages of different modelling methods were discussed.

Kumar *et al.* [17] presented a non-isolated bidirectional multiple input dc-dc converters to interface a battery and an ultra capacitor for vehicular applications. The proposed converter was capable of drawing power from multiple energy sources to supply the demand of vehicle loads. The presented converter has bidirectional capability and operates in buck, boost or buck-boost modes of operation and the proposed converter along with inverter-motor drive was analyzed through detailed device level simulation in open loop modes.

2.3 CONCLUSION

The chapter gives an insight of the developments occurring in power converter topology of hybrid electric vehicles and state space modelling of buck and the boost operation of DC-DC converter. In our next chapter, we are going to discuss the design and analysis of power converter used in hybrid electric vehicle.

CHAPTER 3

DESIGN OF POWER CONVERTER

3.1INTRODUCTION

Power electronics is the important technology responsible to shift from conventional vehicles to electric hybrid and fuel cell vehicles. The chapter discusses the complete system overview of the hybrid vehicle. The complete block diagram representation is given to demonstrate the working of components in power management in HEV. Description of the bidirectional dc-dc operation is discussed. The main focus of the chapter is on the two modes of operation such as in generating mode and in motoring mode. Both modes of operations involve different parameters that need to be calculated.

IGBT and diodes are the major components in a dc-dc converter .These have significant power losses. Both IGBT as well as diode have conduction and switching losses. Conduction losses are more than the switching losses. These losses play significant role in efficiency calculation .Overview of the bidirectional converter in HEV followed by loss calculation in semiconductor loss calculation.

Efficiency of the converter not only dependent on losses in semiconductors but the design of the inductor and capacitor also play crucial role. Core shape and size are other important factors that are to be assumed carefully. Shape and size of the inductors depend on the constraint and voltages applied in the input and the output. Inductor design and the capacitor value at the output and at the input decide the total losses and therefore the efficiency of the converter.

3.2 THE HYBRID ELECTRICAL VEHICLE

Figure 3.1 shows the block diagram of a HEV with a battery directly connected to the inverter and further connected to the electric motor, and in the opposite direction power is

transferred from Load (wheel-motor) to battery through inverter. In the other way the power comes from the generator to the inverter which is connected to the ICE.

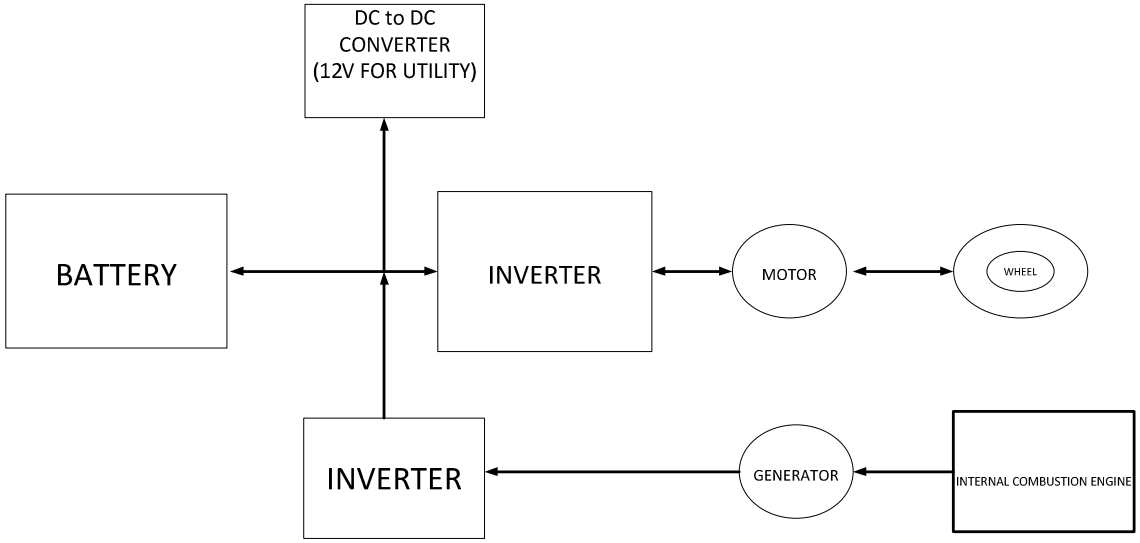

Figure 3.1Block diagram of a HEV without DC-DC converter.

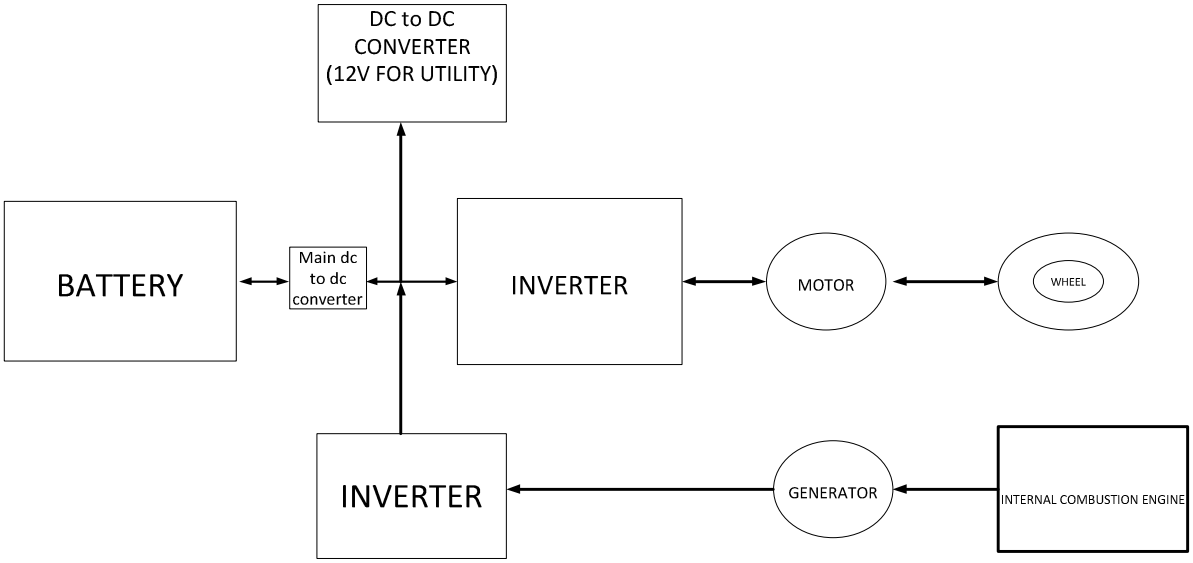

Figure 3.2 Block diagram of a HEV with DC-DC converter.

Figure 3.2 shows the block diagram of a HEV without DC-DC converter. The DC-DC converter in a HEV is used to maintain a constant dc link voltage and to step up and step down the voltage as shown in Figure 3.2.

There are many different potential HEV configurations, but in general a HEV has an electric drive train like an EV, plus an internal combustion engine (ICE) that can charge the batteries periodically as is shown in Figure 3.2. The internal combustion engine is most

efficient for a small range of operating conditions. This is utilized in HEV where the internal combustion engine can be made to operate at this efficient operating point.

The HEV can operate the internal combustion engine (ICE) at its most efficient point for charging of the battery and can use the drive train to take up all the slack under other conditions. The emissions are lower than the combustion engine driving the car by itself and fuel economy can be significantly improved. The usable range of Electrical vehicles can be extended by hybrid technologies. A hybrid would allow the vehicle to operate in an urban/polluted area with only batteries and then switch to the engine outside the urban area.

3.3 BIDIRECTIONAL BOOST CONVERTER

There are generally two bidirectional DC-DC converters in hybrid vehicle applications. One of them is a high-power converter that links the hybrid power train battery at a lower voltage with the high voltage DC bus. A second low-power converter links the hybrid battery with the low voltage auxiliary battery [1]. The operating principle of the DC-DC converter is shown in Figures 3.3.a-c.

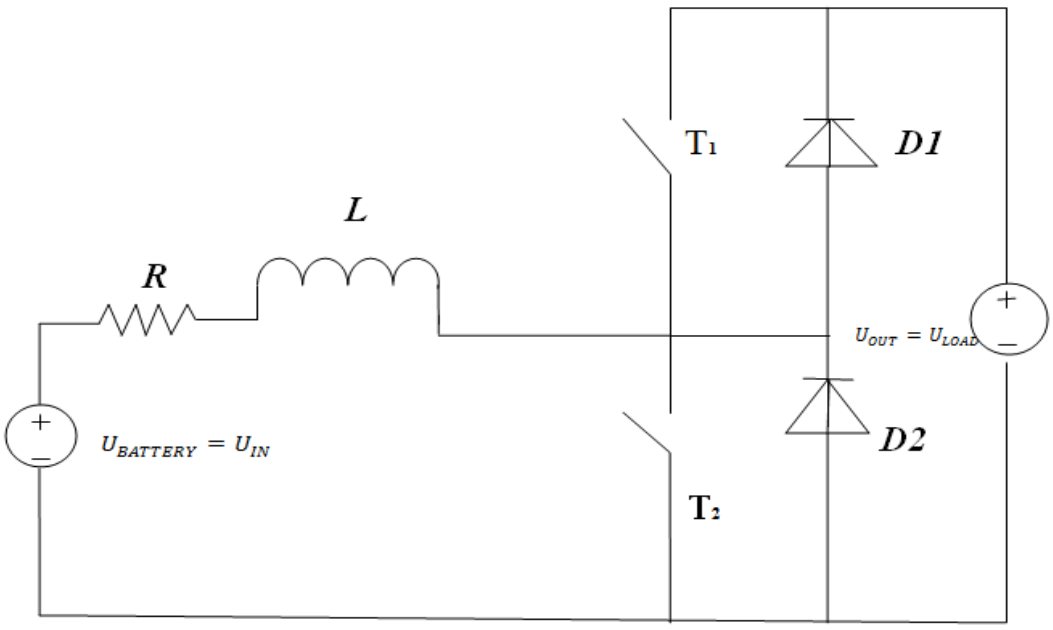

(a) Circuit topology of a bidirectional converter.

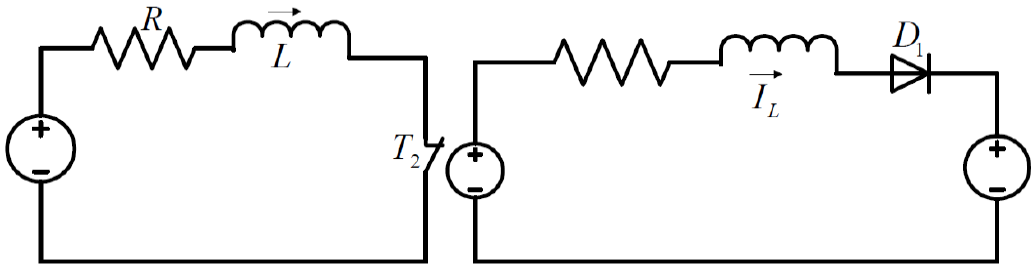

(b) Operating conditions for motoring mode of operation.

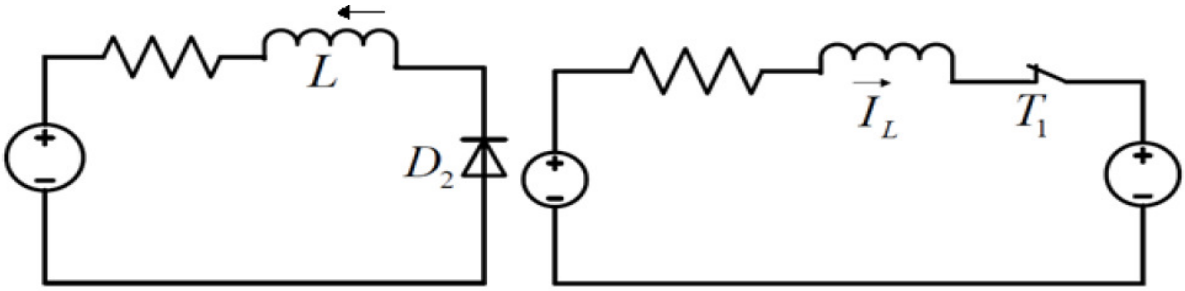

(c) Operating conditions for generating mode of operation

Figure 3.3 Operation of the bidirectional boost converter [2]

In Figures 3.3 b-c shows the motoring and generating mode of a typical DC-DC converter is shown where in motoring mode the power is transferred from the battery to the load and vice versa.

3.3.1 GENERATING MODE

In buck operation, as shown in Figure 1(c), the power is transferred from $\boldsymbol{V_{LOAD}}$ to $\boldsymbol{V_{BATTERY}}$. When $\boldsymbol{T_1}$ is closed and $\boldsymbol{T_2}$ is open, since $\boldsymbol{V_{LOAD}}$>$\boldsymbol{V_{BATTERY}}$, $\boldsymbol{V_L}$ =$\boldsymbol{V_{LOAD}}$ --- $\boldsymbol{V_{BATTERY}}$ and the inductor current $\boldsymbol{I_L}$ builds up. When $\boldsymbol{T_1}$ is open, the inductor current $\boldsymbol{I_L}$ continues to flow through $\boldsymbol{D_2}$ .Thus, $\boldsymbol{V_L = -V_B}$ [2]. Assume ideal components and a constant $\boldsymbol{V_O}$, the inductor current over one cycle in steady state operation will remain the same, e.g.,

$$\int_{0}^{ON}(V_{BATTERY} - V_{DC\ Link})dt = \int_{t1_{ON}}^{t1_{ON}-t2_{OFF}}(-V_{DC\ Link}) \quad (3.1)$$

$$V_O = \frac{t1_{ON}}{T}V_{BATTERY} = K_1 V_{BATTERY} \quad (3.2)$$

where K_1 is the duty ratio defined as the percentage of on-time of switchT_1.

3.3.1.1. PARAMETERS FOR LOSS CALCULATION:

Figure 3.4 shows the typical signals in the step down (buck) converter. Input parameters for the calculation: Input voltage ($U_{IN} = V_{BATT.}$), output voltage ($U_O = V_{LOAD}$), output power (P_O), inductor value (L), switching frequency (f_{SW}) [20].

The output current of the converter is

$$I_O = \frac{P_O}{Q_O} \tag{3.3}$$

The duty cycle in continuous conduction mode is

$$K = \frac{U_O}{U_{IN}} \tag{3.4}$$

The output current ripple is

$$\Delta I_0 = \frac{(1-K)}{L} U_O \tag{3.5}$$

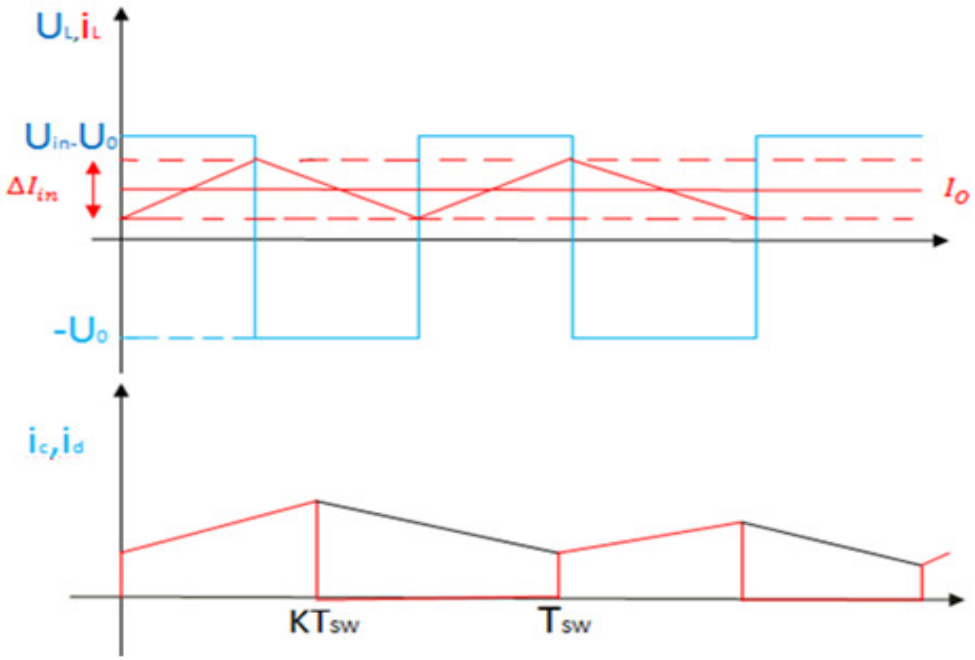

Figure 3.4.Inductor voltage, current, diode and capacitor current signals in generating mode. [20]

In Figure 3.4 shows the typical signals of inductor voltage, inductor current, capacitor current, diode current input and output voltages. The parameters needed for the loss calculation can be determined as

$$\boldsymbol{I_{CON} = I_O - \frac{\Delta I_O}{2}} \tag{3.6}$$

$$\boldsymbol{I_{COFF} = I_O + \frac{\Delta I_O}{2}} \tag{3.7}$$

$$\boldsymbol{I_{CAV} = KI_O} \tag{3.8}$$

$$\boldsymbol{I_{DRMS} = (1 - K)I_O^2} \tag{3.9}$$

3.3.2 MOTORING MODE

In this operation, the power is transferred from $\boldsymbol{V_{BATTERY}}$ to $\boldsymbol{V_{DC\ Link}}$.When $\boldsymbol{T_2}$ is closed and $\boldsymbol{T_1}$ is open, the output voltage capacitor and inductor form a direct path through switch $\boldsymbol{T_2}$ as shown in figure 3.3(a) and figure 3.3(b). Therefore, $\boldsymbol{V_L = V_{BATTERY}}$ and the inductor current $\boldsymbol{I_1}$ builds up [2]. When $\boldsymbol{T_1}$ is open, the inductor current continues to flow through$\boldsymbol{D_1}$ to $\boldsymbol{V_D}$, therefore

$$\boldsymbol{V_L = V_{DC\ Link} - V_{BATTERY}} \tag{3.10}$$

Assume ideal components and a constant $\boldsymbol{V_D}$ the inductor current over one cycle in steady statewill remain the same, e.g.

$$\boldsymbol{\int_0^{t2_{ON}} (V_{DC\ Link})dt = (V_{BATTERY} - V_{DC\ Link})dt} \tag{3.11}$$

$$\boldsymbol{V_{DC\ Link} = \frac{1}{1-K} V_{BATTERY}} \tag{3.12}$$

where $\boldsymbol{K}$ is the duty ratio defend as the percentage of the on-time of switch $\boldsymbol{T_2}$.

$$\boldsymbol{K = \frac{t_{2ON}}{T}} \tag{3.13}$$

3.3.2.1 PARAMETERS FOR LOSS CALCULATION: Figure 3.5 shows the typical signals in the step up (boost) converter [20]. Input parameters for the calculation: Input voltage($\boldsymbol{U_{IN} = V_B}$), output voltage ($\boldsymbol{U_{OUT} = V_D}$), output power ($\boldsymbol{P_O}$), inductor value ($\boldsymbol{L}$), switching frequency ($\boldsymbol{f_{SW}}$).

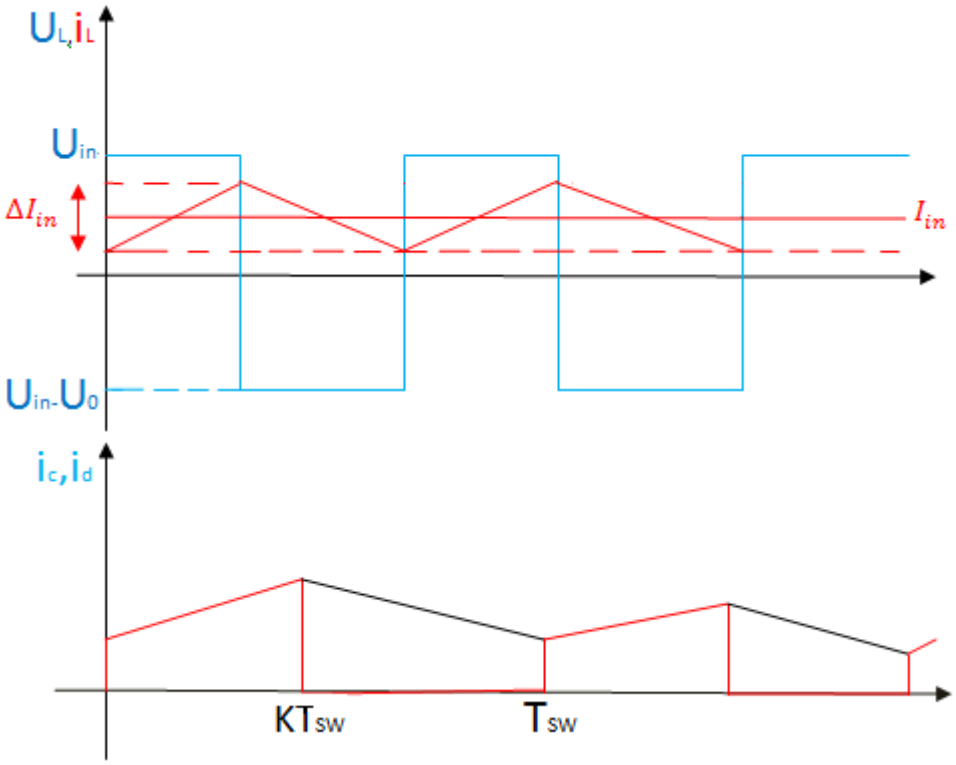

Figure 3.5.Inductor voltage, current, diode and capacitor current signals in motoring mode [19].

The input current is

$$\boldsymbol{I_{IN} = \frac{P_{IN}}{U_{IN}}} \tag{3.14}$$

where the duty cycle in continuous conduction mode is found to be

$$\boldsymbol{K = 1 - \frac{U_{IN}}{U_O}} \tag{3.15}$$

The input current ripple is

$$\boldsymbol{\Delta I_{IN} = \frac{KU_{IN}}{Lf_{SW}}} \tag{3.16}$$

The parameters needed for the loss calculation can be determined as

$$I_{CON} = I_{IN} - \frac{\Delta I_{IN}}{2} \quad (3.17)$$

$$I_{COFF} = I_{IN} + \frac{\Delta I_{IN}}{2} \quad (3.18)$$

$$I_{CAV} = KI_{IN} \quad (3.19)$$

$$I_{RMS}^2 = (1-K)I_{IN} \quad (3.20)$$

$$I_{DAV} = (1-K)I_{IN} \quad (3.21)$$

$$I_{DRMS}^2 = (1-K)I_{IN}^2 \quad (3.22)$$

3.4 SEMICONDUCTOR LOSS CALCULATION OF THE CONVERTER

The bidirectional dc-dc converter has IGBT and diodes as the major components. These devices have significant power loss. Both IGBT as well as diode have conduction and switching loss during operation. Thus, these losses need to be discussed to know the total converter loss contribution due to semiconductor devices.

3.4.1 IGBT AND DIODE LOSSES

The IGBT and diode power losses as well as the power losses in any semiconductor component can be divided in three groups [19]:

a) Conduction losses ($P_{CONDUCTION}$)

b) Switching losses (P_{SW})

c) Blocking leakage losses usually neglected

Therefore

$$P_{SEMICONDUCTOR} = P_{CONDUCTION} + P_{SW}$$

3.4.1.1 CONDUCTION LOSSES

(A) IGBT CONDUCTION LOSSES: The IGBT conduction losses can be calculated using an IGBT voltage drop behaviour approximation with a series connection of a DC voltage source

representing the IGBT on state zero current collector emitter voltage and collector on state resistance ($\boldsymbol{r_C}$) as

$$\boldsymbol{u_{CE}\,(i_C) = \; u_{CEO} + r_c i_c} \tag{3.23}$$

The important parameters can be read directly from the IGBT datasheet .The $\boldsymbol{u_{CEO}}$and values can be read from the diagram. The instantaneous value of the IGBT conduction losses are

$$\boldsymbol{P_{CT}(t) = u_{CE}(t) i_c(t) = u_{CEO} i_C(t) + r_C i_C^2(t)} \tag{3.24}$$

The average IGBT current value is $\boldsymbol{I_{CAV}}$ and value of IGBT current is$\boldsymbol{I_{CRMS}}$. Then the average power losses can then be expressed as

$$\boldsymbol{P_{CT}(t) = \frac{1}{T_{SW}} \int_0^{T_{SW}} p(t)\, dt = \frac{1}{T_{SW}} \int_0^{T_{SW}} \left(u_{CEO} i_C(t) + r_C i_C^2(t) dt\right)}$$

$$\boldsymbol{= \quad u_{CEO} i_{CAV} + r_C I_{CRMS}^2} \tag{3.25}$$

(B) DIODE CONDUCTION LOSSES: The same approximation can be used for the anti-parallel diode as is used for IGBT, giving

$$\boldsymbol{u_D(i_D) = u_{DO} + r_D i_D} \tag{3.26}$$

The instantaneous value of the diode conduction losses is

$$\boldsymbol{P_{CD}(t) = u_D(t) i_D(t) = u_{DO}(t) i_D(t) + r_D i_D^2} \tag{3.27}$$

If the average diode current is $\boldsymbol{I_{DAV}}$ and the rms diode current is $\boldsymbol{I_{DRMS}}$, the average diode conduction losses across the switching period ($\boldsymbol{\frac{1}{f_{SW}}}$) are

$$\boldsymbol{P_{CD}(t) = \frac{1}{T_{SW}} \int_0^{T_{SW}} (u_{DO} i_D(t) + r_D i_D^2(t)\, dt) u_{DO} I_{DAV} + r_D I_{DRMS}^2} \tag{3.28}$$

The value of $\boldsymbol{u_{CEO}}$and $\boldsymbol{u_{DO}}$ can be read from the datasheet as following .The$\boldsymbol{r_C}$ and $\boldsymbol{r_D}$values can also be calculated from the datasheet by taking the slope of the desired line of characteristics as shown in Figure 3.6.

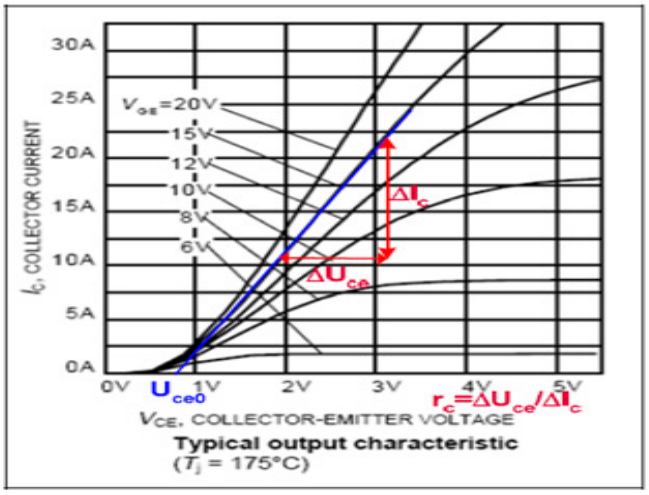

Reading the u_{CE0} and r_C ($r_C = \Delta U_{ce}/\Delta I_c$) from the data-sheet diagram

Figure 3.6.The graph of a transistor to read the initial voltage and resistance values [20].

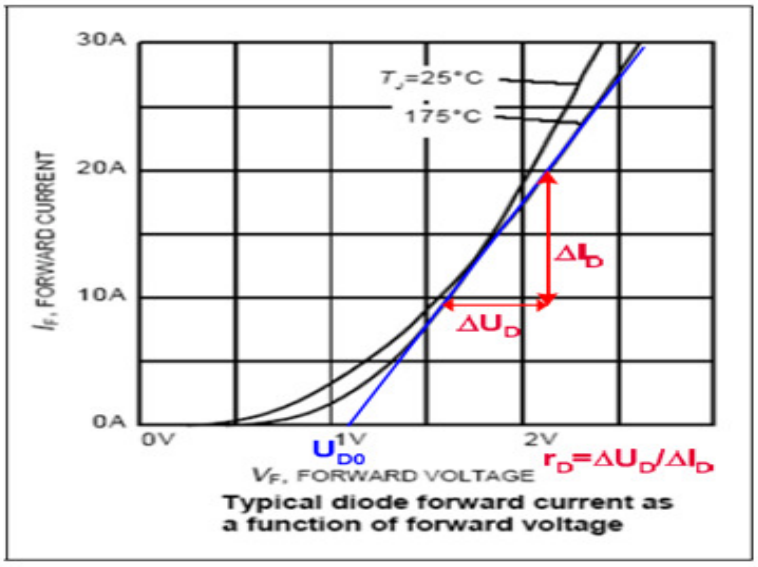

Figure 3.7 The graph of a diode to read the initial voltage and resistance values [20].

3.4.1.2 SWITCHING LOSSES

The switching losses in the IGBT and the diode are the product of the switching energies and the switching frequency f_{SW}.

$$P_{SWM} = (E_{ONM} + E_{OFFM}) f_{SW} \quad (3.29)$$

$$P_{SWD} = (E_{OND} + E_{OFFD}) f_{SW} \quad (3.30)$$

where the energy during on and off period can be written as

$$E_{ONM} = E_{REFON} \frac{\Delta V_{IN}}{V_{REFON}} \frac{I_{IN}}{I_{REF}} \quad (3.31)$$

$$E_{OFFM} = E_{REFOFF} \frac{\Delta V_{IN}}{V_{REF}} \frac{I_{IN}}{I_{REF}} \quad (3.32)$$

Where V_{REF} and I_{REF} are taken from datasheet of IGBT [23] and ΔV_{IN} and I_{IN} are the output voltage and current respectively. E_{REFON} and E_{REFOFF} can be calculated from the following typical switching losses of the IGBT according to Figure 3.8. Figure 3.8 show how to read the values of energies E_{ONM} and E_{OFFM} can be read from a given datasheet respective current level.

The turn on energy in the diode consists mostly of the reverse recovery energy (E_{OND}).

$$E_{OND} = \frac{1}{4} Q_{RR} U_{DRR} \quad (3.33)$$

Where U_{DRR} is the voltage across the diode during reverse recovery .The Q_{RR} and U_{DRR} are taken from the datasheet of the IGBT.

Total losses

$$P_T = P_{CT} + P_{SWT} = u_{CEO} I_{CAV} + r_C I_{CRMS}^2 + (E_{ONT} + E_{OFFT}) f_{SW} \quad (3.34)$$

$$P_D = P_{CD} + P_{SWD} = u_{DO} I_{DAV} + r_D I_{DRMS}^2 + E_{OND} f_{sw}$$

Typ. switching losses

$E = f(I_C)$, inductive load , T_j = 125°C

par.: V_{CE} = 600 V, V_{GE} = ± 15 V, R_G = 4.7 Ω

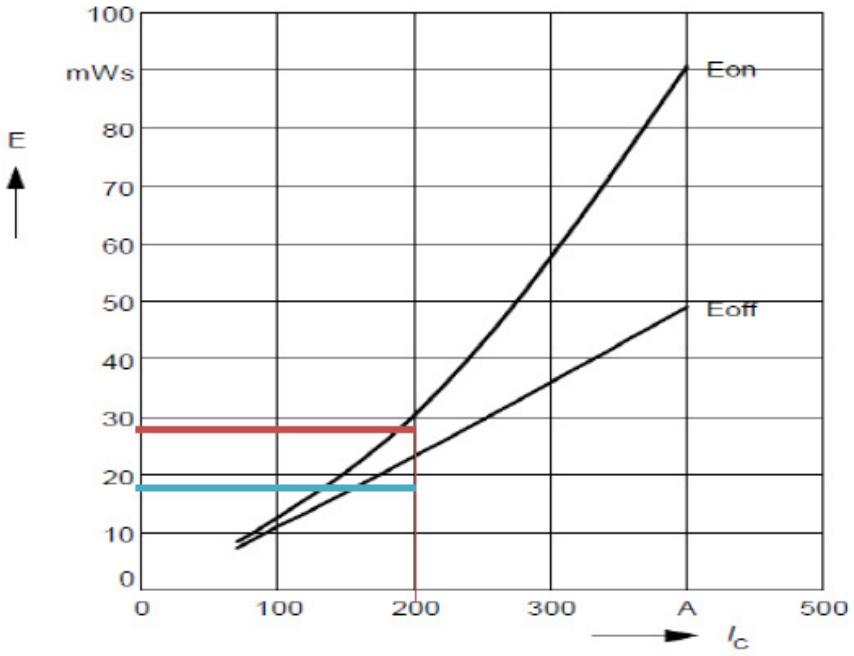

(3.35)

Figure 3.8 Graph of a transistor to read energy values[20].

During charging, an external electrical power source (the charging circuit) applies higher voltage (but of the same polarity) than that produced by the battery, forcing the electrical current to pass in the reverse direction. The lithium ions then migrate from the positive to the negative electrode, where they become embedded in the porous electrode material in a process known as intercalation.

3.5 INDUCTOR AND CAPACITOR DESIGN

After having the losses known in the semiconductor devices, we need to design the core of the inductor .The core chosen is not taken by choice. There are some constraints some issues that are going to be discussed here. Inductors are not commercially available and therefore need to be designed according to our requirement. In, this chapter, an inductor is designed. A carefully considered power inductor is often a key design element to achieve a small, efficient, and cost effective converter.

For many inductor applications, powder cores are clearly superior compared with alternative core materials, such as ferrites or steel laminations. The designer has many choices in powder core materials and shapes, each offering trade-offs among loss performance, cost, size, and ease of winding. In addition, as the design criteria change, so do the benefits and shortcomings of each particular core material. An understanding of the advantages and disadvantages involved is necessary for making good choices [18].

3.5.1 DESIGN OF THE INDUCTOR

Parameters:

The average current of the Inductor

$$I_{AVG} = \frac{P}{\Delta V_{IN}} \tag{3.36}$$

The ripple current can be calculated as

$$\Delta I = \frac{I_{MAX} - I_{MIN}}{2} \tag{3.37}$$

where maximum and minimum currents can be calculated as

$$I_{MAX} = I + \frac{0.2I}{2} \text{ and } I_{MIN} = I - \frac{0.2I}{2}$$

3.5.1.1 CORE MATERIALS

FERRITE CORE: Ferrites are manufactured from raw material are oxides of various metals such as iron, manganese, and zinc. Ferrites have high resistivity than manganese alloys, enabling them to function at much higher frequencies, even at the high frequency region. The raw materials are generally mixed at fired in kiln. Then they are broken into uniform particles, and pressed into one of many shapes. There is another atmosphere controlled sintered kiln for firing of “green” cores. Sintered cores are a hard ceramic; therefore further processing has to be done with diamond grinding wheels [19].

IRON POWDER CORE: Molypermalloy Powder cores are made from an iron, nickel and molybdenum alloy powder exhibiting the lowest core loss of the powder core materials, but has the high processing costs and its high nickel content. MPP toroids are available from 3.5 mm to 125 mm in outside diameter. High Flux cores are alike Molypermalloy powder core, made from a nickel-iron alloy powder. Containing 50% nickel, High Flux pricing is cheaper than MPP. High Flux has higher

core loss than MPP and Kool Mμ, but due to its higherB_{SAT}, High Flux performance in best in permeability vs. bias. High Flux is not widely available in shapes other than toroids.
Kool Mμ, also known as "sendust" distributed air gap cores made from an iron, aluminium, silicon alloy powder. The Kool Mμ material is similar to DC bias performance with MPP.

Kool Mμ is much more economical than the MPP due to the absence of nickel in the formulation. However, Kool Mμ has higher AC losses than MPP. It is designed to be a practical alternative when iron powder is too lossy, typically because the frequency is moderate or high, but MPP is too expensive. In addition to toroids, KoolMμ is available in E-core shapes, so that winding costs may be minimized as well. Iron powder cores have higher core losses than MPP, High Flux, or KoolMμ, but are generally less expensive. Iron powder is often the best choice for a power inductor when the highest efficiency and smallest size are not required, but cost is critical; or when the frequency is quite low; or when the amplitude of the AC ripple current is very low (resulting in very low AC flux, and thus reasonably low AC losses.)

An organic binder, for the grain-to-grain insulation, is present in most iron powder cores that is susceptible to breakdown over time under high temperature operation. So the designer may need to take account of the thermal aging curves for the iron powder material being considered. There is a moderate pressing densities for iron powders and therefore there are variety of shapes for the materials including toroids, E-cores, pot cores, U-cores, and rods.

.

3.5.1.2 CORE SHAPES

ETD CORES: ETD cores have been designed to make optimum use of a given volume of ferrite material for maximum throughput power, specifically for forward converter transformers. The structure, which includes a round centerpost, approaches a nearly uniform cross-sectional area throughout the core and provides a winding area that minimizes winding losses. ETD cores are used mainly in switched-mode power supplies and permit off-line designs where IEC and VDE isolation requirements must be met.

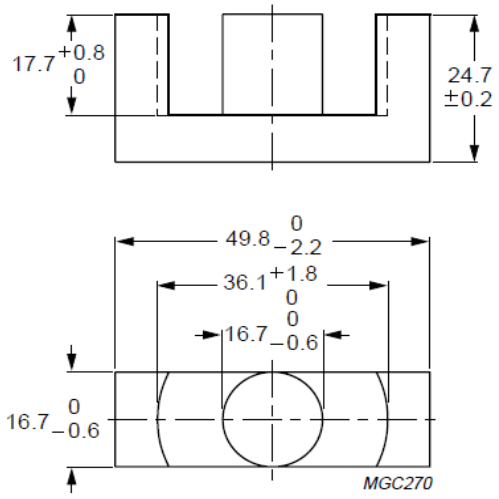

Figure 3.9 ETD-49 Core.[21]

EC CORES: These shapes are a cross between E cores and pot cores. Like E cores, they provide a wide opening on each side that gives adequate space for the large size wires required for low output voltage switched mode power supplies. It also allows for a flow of air which keeps the assembly cooler. The centerpost is round, like that of the pot core. Winding in the round centerpost has a shorter path length around it than the wire around a square centerpost with an equal area thereby reduces the losses of the winding by 11% enabling the core to handle a high output power. The round centerpost also removes the sharp bend in the wire that occurs with winding on a square centerpost.

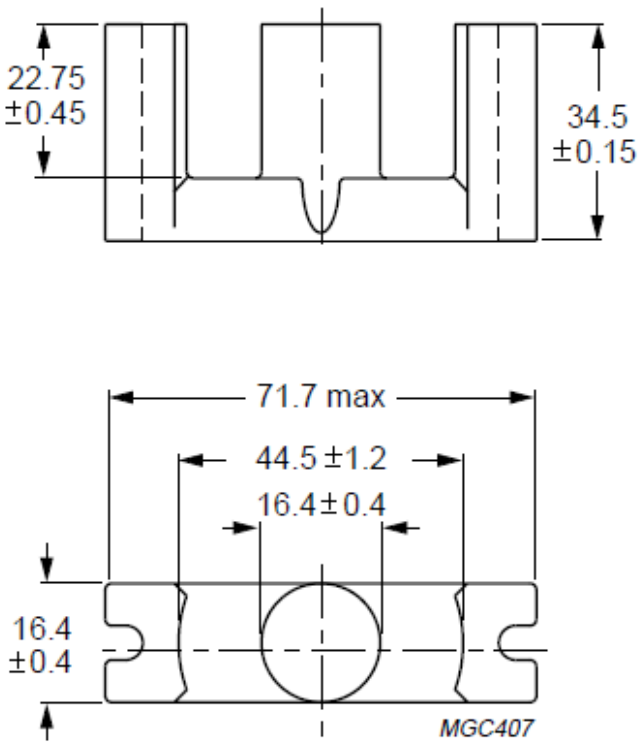

Figure 3.10 EC-70 Core. [22]

where switching frequency = $\boldsymbol{f}$(Hz)

Inductance of the inductor = $\boldsymbol{L}$(μH)

$$\boldsymbol{Z_{INDUCTOR} = 2\pi fL} \tag{3.38}$$

$$\boldsymbol{NI = \Phi R = \frac{\Psi}{N} R} \tag{3.39}$$

$$\boldsymbol{NI = \frac{\Psi}{I} = \frac{N^2}{R}} \tag{3.40}$$

Effective area in square meters is = $\boldsymbol{A_e}$

Effective length in meters is = $\boldsymbol{l_e}$

Relative permeability of the material = $\boldsymbol{\mu_r}$

Permeability constant = $\boldsymbol{\mu_o}$

Current density = $\boldsymbol{J}$ (A/mm^2)

Reluctance for the iron part

$$\boldsymbol{R_{fe} = \frac{l_e}{(\mu_o \mu_r \, A_e)}} \tag{3.41}$$

where, air gap for coil = $\boldsymbol{l_{air}}$

Reluctance for the air gap

$$\boldsymbol{R_{air}} = \frac{\boldsymbol{l_{air}}}{(\boldsymbol{\mu_0 \mu_r A_e})} \tag{3.42}$$

The required number of turns

$$\boldsymbol{N} = \sqrt{\boldsymbol{LR}} \tag{3.43}$$

Total reluctance must be

$$\boldsymbol{R} = \boldsymbol{R_{fe}} + \boldsymbol{R_{air}} \tag{3.44}$$

The total flux in the core can be calculated as

$$\boldsymbol{\Phi} = \frac{\boldsymbol{NI}}{\boldsymbol{R}} \tag{3.45}$$

The iron losses

$$\boldsymbol{P_{fe}} = \boldsymbol{l_{factor} l_e A_e} \tag{3.46}$$

where , loss factor is obtained from datasheet.

Copper resistance

$$\boldsymbol{R_{Cu}} = \frac{\boldsymbol{l_W}}{\boldsymbol{A_c}} \tag{3.47}$$

Winding length

$$\boldsymbol{l_w} = \boldsymbol{N L_w} \tag{3.48}$$

where turn length can be found from datasheet.

Copper losses

$$\boldsymbol{P_{Cu}} = \boldsymbol{R_{Cu} I_{IN}^2} \tag{3.49}$$

Total inductor losses

$$= \boldsymbol{P_{fe}} + \boldsymbol{P_{Cu}} \tag{3.50}$$

3.6 DESIGN OF CAPACITORS

3.6.1 INPUT CAPACITOR (C_{Input}):

The C_{Input} can be calculated by the following formula

$$C_{Input} = \frac{\Delta I_L T_{SW}}{8\Delta V_O} \tag{3.51}$$

where ΔV_O peak-to-peak voltage ripple of the buck converter output (1 to 2 % of the output voltage).

3.6.2 OUTPUT CAPACITOR (C_{Output}):

The C_{Output}can be calculated by the following formula

$$C_{Output} = \frac{I_O K T_{SW}}{\Delta V_O} \tag{3.52}$$

where ΔV_O is peak-to-peak voltage ripple of the boost converter output (1 to 2 % of the output voltage).

3.7 CONCLUSION

Bidirectional flow of energy plays a significant role in the functioning and importance of Hybrid Vehicles system. Operations of the converter in both directions explained. Functioning of the converter involves losses in the semiconductor devices such as IGBT and diode that are calculated. After the overview and calculation of losses in the converter, their needed to implement that methodology in case study. According to given parameters and losses calculation, taking into consideration different core shape and material, converters are designed. Designed converter is to be analysed using bode plot and their corresponding poles location are to be checked, which can be made possible by developing state space averaging model.

CHAPTER 4

CASE STUDY

4.1 INTRODUCTION

In the previous chapter we came across the design methodology of dc-dc converter hybrid electric vehicles. The different core shapes and core materials are discussed. In this chapter, we have taken up the design of the dc-dc converter. The methodology depicted earlier is now being implemented for material and shape of the inductor taken up for design.

4.2 DESIGN

The different inductor types considered for this work are given as follows:

1. Ferrite EC-70
2. Ferrite ETD-49
3. Iron powder EC-70
4. Iron powder ETD-49

Given below are the specifications required to carry out the design.

$\boldsymbol{P_O = 60KW}$

$\boldsymbol{V_{INMIN} = 300V}$

$\boldsymbol{V_{INMAX} = 450V}$

$\boldsymbol{V_O = 450V}$

$\boldsymbol{f_{SW} = 20KHz}$

$\boldsymbol{l_{AIR} = 10mm}$

$\boldsymbol{Current\ density(J) = (3\ A/mm^2)}$

4.2.1 CORE SHAPES:

CORE SHAPE	Cross sectional area(A_e)	Magnetic path length (L_e)	Mean length per turn (L_w)
EC-70	2.79 sq.cm	14.4 cm	12.9 cm
ETD-49	2.11 sq.cm	11.4 cm	8.51 cm

4.2.2 CORE MATERIALS [19]:

Ferrite: Relative permeability = 5000

Iron powder: Relative permeability = 71

Parameters used for loss calculations:

1.$r_c = 0.0076$,$r_D = 0.0015$

2.$U_{CEO} = 1.13$, $U_{DO} = 0.75$

3.$E_{REFON} = 6.5mJ$

4.$E_{REFOFF} = 11mJ$

5.$E_{ONT} = 0.0043$

6.$E_{OFFT} = 0.0073$

7.$E_{OND} = 0.0047$

8.$E_{OFFD} \sim 0$

4.3 RESULTS

Results for the designed converters can be tabulated as follows

	MOTORING MODE		GENERATING MODE	
CORE	Losses	Efficiency	Losses	Efficiency
Ferrite EC-70	597.49	99.00	644.14	98.92
Ferrite ETD-49	594.04	99.01	640.70	98.93
Iron powder EC-70	656.85	98.91	703.51	98.83
Iron powder ETD-49	636.12	98.94	682.87	98.86

4.4 CONCLUSION

In this work, DC-DC converter is investigated with different core materials, core shapes, at (450 V) and 20 kHz for an EV/BEV/HEV. The efficiency of the converter is higher for a ferrite material .The 450V system is better with ferrite core material. The designed converters need to be analysed using frequency domain analysis. For that purpose state space averaging modelling for both buck and boost operation are to be developed.

CHAPTER 5

ANALYSIS OF POWER CONVERTER

5.1 INTRODUCTION

State space averaging approximates the time variant system with a linear continuous time invariant system. Converter is basically a switching between different time invariant systems during each switching period and is therefore, a time variant system. State space averaging is presented to derive model of buck converter followed by model of boost converter. Design oriented analysis taken into account the way disturbances and changes in the input and control signals affect the optimum performance of these converters. Line to output transfer function determination describes how change in the applied voltages lead to change in output voltage. Control to output transfer function describes how control input variation affects the output voltages. Similarly input and output impedances of converter play an important role when EMI filter is added to converter.

5.2 STATE SPACE AVERAGING

The converter behaves as a time invariant system while transistor is ON. For other time period when the transistor is OFF, converter again acts as a time invariant system. Therefore, converter can described as switching between time invariant systems during the switching period. If transistor is switched like this, it behaves as switching between different time invariant systems during the switching period. Consequently converter can be modelled as time variant system. State-space averaging given by Middle brook and Cuk in the year 1976 is one of the method that approximates this time invariant with a linear continuous time invariant system .This methodology involves the state-space description as this method uses the state space in each time invariant system as a starting point. These are then averaged on

basis of their duration. Models are finally linearized at operating point to obtain a small signal model to extract three transfer functions: 1.The control-to-output transfer function 2.The output impedance 3.The audio susceptibility.

5.3 MODELLING OF BIDIRECTIONAL OPERATION

5.3.1 MODEL OF BUCK CONVERTER

During the time in which transistor is on the voltage across diode equals the input voltage. Circuit in figure 5.1 can be therefore used as model of buck converter during time intervalt_{on}. Current source is added which injects current in output stage .This current is therefore an input signal [4].

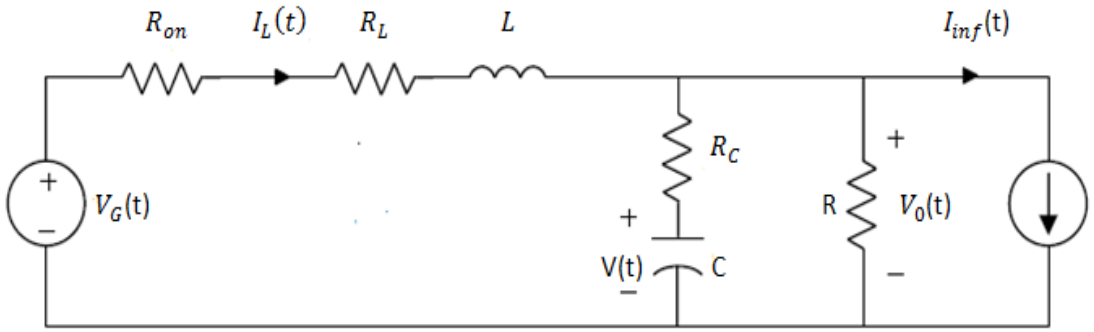

Figure 5.1 Circuit of the buck converter during t_{on}

$$V_G(t) - I_L(t)(R_L + R_{on}) - L\frac{dI_L}{dt} = V_O(t) \tag{5.1}$$

$$\frac{V_G(t)-V_O(t)}{L} - \left(I_L(t)\frac{(R_L+R_{on})}{L}\right) = \frac{dI_L(t)}{dt} \tag{5.2}$$

$$\frac{dI_L}{dt} = -I_L\frac{R_L+R_{on}}{L} + \left(\frac{V_G(t)-V_o(t)}{L}\right) \tag{5.3}$$

$$C\frac{dV(t)}{dt} = I_L(t) - \frac{V_o(t)}{R} - I_{inj}(t) \quad (5.4)$$

Equation 5.2 rearranged to give

$$V_o(t)\left(1 + \frac{R_C}{R}\right) = V(t) + R_c\left(I_L(t) - I_{inj}(t)\right) \quad (5.5)$$

$$V_O(t) = \frac{R\,R_C}{R+R_C}I_L(t) + \frac{R}{R+R_C}V(t) - \frac{R\,R_C}{R+R_C}I_{inj}(t\,) \quad (5.6)$$

$$\frac{dI_L}{dt} = \left(-\frac{R_L+R_{on}}{L} - \frac{R\,R_C}{(R+R_C)L}\right)I_L(t) - \frac{R}{(R+R_C)L}V(t) + \frac{V_O(t)}{L} + \frac{RR_C}{(R+R_C)L}I_{inj}(t) \quad (5.7)$$

$$\frac{dV(t)}{dt} = \frac{1}{C}I_L(t) - \frac{R_C}{(R+R_C)C}I_L - \frac{1}{(R+R_C)C}V(t) + \frac{R}{(R+R_C)C}I_{inj} - \frac{1}{C}I_{inj}(t) \quad (5.8)$$

Circuit is a second order system. Let $I_L(t)$ and V(t) be the state variable.$V_G(t)$ and $I_{inj}(t)$ be the input signals and $V_O(t)$ as the output signals. From the above equations, state space models can be obtained as follows:

$$\frac{dx(t)}{dt} = A_1x(t) + B_1u(t) \quad (5.9)$$

$$y(t) = C_1x(t) + F_1u(t) \quad (5.10)$$

where

$$\text{x(t)}=\begin{bmatrix} I_L(t) \\ I_{inj}(t) \end{bmatrix} \quad (5.11)$$

$$\text{u(t)}=\begin{bmatrix} V_G \\ I_{inj}(t) \end{bmatrix} \quad (5.12)$$

$$\text{y(t)}=[V_O(t)] \quad (5.13)$$

$$A_1 = \begin{bmatrix} -\frac{R_L}{L} - \frac{R\,R_C}{(R+R_C)L} & -\frac{R}{(R+R_C)L} \\ \frac{R}{(R+R_C)C} & -\frac{1}{(R+R_C)C} \end{bmatrix} \quad (5.14)$$

$$B_1 = \begin{bmatrix} \frac{1}{L} & \frac{RR_C}{(R+R_C)L} \\ 0 & \frac{-R}{(R+R_C)C} \end{bmatrix} \quad (5.15)$$

$$C_1 = \begin{bmatrix} \frac{RR_C}{R+R_C} & \frac{R}{R+R_C} \end{bmatrix} \quad (5.16)$$

$$F_1 = \begin{bmatrix} 0 & -\frac{RR_C}{R+R_C} \end{bmatrix} \quad (5.17)$$

Similarly when the transistor is off, diode voltage goes zero. Figure 5.2 can be used as a circuit for model during interval t_{off}.Therefore state space model can be obtained as follows

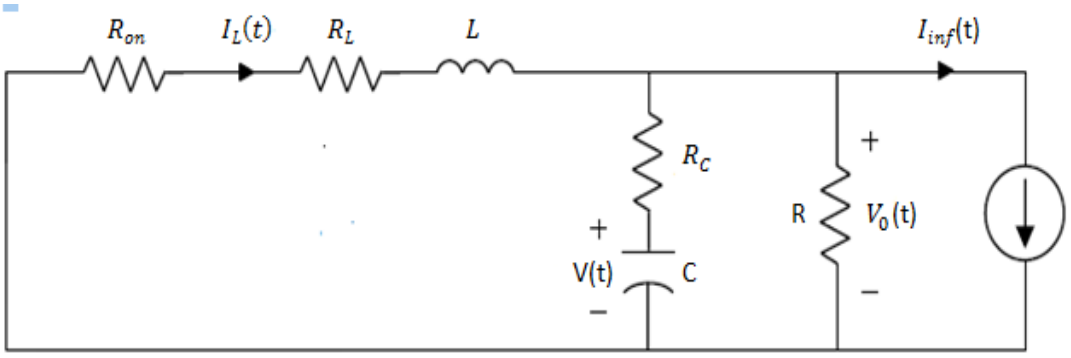

Figure 5.2 Circuit of buck operation during t_{off}

$$\frac{dx(t)}{dt} = A_2x(t) + B_2u(t) \quad (5.18)$$

$$y(t) = C_2x(t) + F_2u(t) \quad (5.19)$$

Where $$A_2 = A_1 \quad (5.20)$$

$$B_2 = \begin{bmatrix} 0 & \frac{RR_C}{(R+R_C)L} \\ 0 & -\frac{R}{(R+R_C)C} \end{bmatrix} \quad (5.21)$$

$$C_2 = \begin{bmatrix} \frac{RR_C}{(R+R_C)} & \frac{R}{(R+R_C)} \end{bmatrix} \quad (5.22)$$

$$F_2 = \begin{bmatrix} 0 & -\frac{R\,R_C}{R+R_C} \end{bmatrix} \quad (5.23)$$

Therefore,

$$A_2 = A_1 \quad (5.24)$$

$$C_2 = C_1 \quad (5.25)$$

$$F_2 = F_1 \quad (5.26)$$

5.3.1.1 METHOD OF STATE SPACE AVERAGING

Converter is basically a switching between two different time invariant system and so it look like time variant system. To approximate this time variant system into continuous time time-invariant system, state space averaging technique is used. In this first calculate the non linear time invariant system by means of averaging followed by linearizing this non linear system.

Two systems are first averaged with respect to their duration in the switching period as:

$$\frac{dx(t)}{dt} = (d(t)A_1 + (1 - d(t))A_2)x(t) + \big(d(t)B_1 + \big(1 - d(t)\big)B_2\big)u(t)$$

$$y(t) = \big(d(t)C_1 + \big(1 - d(t)\big)C_2\big)x(t) + (d(t)E_1 + (1 - d(t))E_2)u(t) \quad (5.27)$$

$$u'(t) = \begin{bmatrix} u(t) \\ d(t) \end{bmatrix} \quad (5.28)$$

In system theory all input are to be placed in input vector and therefore d(t) is placed in input vector.

A nonlinear time-invariant system with state-vector **x**(*t*) , input vector **u'**(*t*) , and output vector **y**(*t*) , are written as

$$\frac{dx(t)}{dt} = f(x(t), u'(t)) \tag{5.29}$$

$$y = g(x(t), u'(t)) \tag{5.30}$$

A straight forward linearizing is now applied where deviation from operating point is as follow

$$x(t) = X + \hat{x}(t) \tag{5.31}$$

$$u'(t) = U + \hat{u}(t) \tag{5.32}$$

$$y(t) = Y + \hat{y}(t) \tag{5.33}$$

Here capital letters denote dc values and hat symbol ($\hat{r}$) denoting the perturbation signals (ac disturbance)**.**

Assume operating point to be in equilibrium i.e.

$$f(x(t), u'(t))\,|_{\substack{x(t)=X \\ u'(t)=U'}} = 0 \tag{5.34}$$

The operating point output values are

$$Y = g\big(x(t), u'(t)\big)\,|_{\substack{x(t)=X \\ u'(t)=U'}} \tag{5.35}$$

Following ac signals can now be obtained as follows:

$$\frac{d\dot{x}(t)}{dt} = A'\hat{x}(t) + B'\hat{x}(t) \tag{5.36}$$

$$\hat{y}(t) = C'\hat{x}(t) + F'\hat{x}(t)$$

Where

$$A' = \left[\frac{\partial f}{dx}\right]_{\substack{x(t)=X \\ u'(t)=U'}} \tag{5.37}$$

$$B' = \left[\frac{\partial f}{du'}\right]_{\substack{x(t)=X \\ u'(t)=U'}} \tag{5.38}$$

$$C' = \left[\frac{dg}{dx}\right]_{\substack{x(t)=X \\ u'(t)=U'}} \tag{5.39}$$

$$F' = \left[\frac{dg}{du'}\right]_{\substack{x(t)=X \\ u'(t)=U'}} \tag{5.40}$$

5.34 and 5.35 can be written as

$$0 = AX + BU \tag{5.41}$$

$$Y = CX + FU \tag{5.42}$$

where

$$A' = DA_1 + DA_2 \tag{5.43}$$

$$B = DB_1 + D'B_2 \tag{5.44}$$

$$C = DC_1 + D'C_2 \tag{5.45}$$

$$F = DF_1 + D'F_2 \tag{5.46}$$

Therefore using above equations, we get

$$A' = A \tag{5.47}$$

$$B_d = B[A_1 - A_2]X + [B_1 - B_2]U \tag{5.48}$$

$$C' = C \tag{5.49}$$

$$F_d = F[C_1 - C_2]X + [F_1 - F_2]U \tag{5.50}$$

$$\frac{d\dot{x}(t)}{dt} = A'\hat{x}(t) + B'\hat{x}(t) \quad (5.51)$$

$$\hat{y}(t) = C'\hat{x}(t) + F'\hat{x}(t) \quad (5.52)$$

$$B' = [B \;\; B_d] \quad (5.53)$$

$$F' = [F \;\; F_d] \quad (5.54)$$

Extraction of transfer functions from state space averaging:

Using 5.43, 5.45, 5.53, 5.54 in equations

$$s\hat{x}(s) = A\hat{x}(s) + B'\hat{u}'(s) \quad (5.55)$$

$$\hat{y}(s) = C\hat{x}(s) + F'\hat{u}'(s) \quad (5.56)$$

$$\hat{x}(s) = (sI - A)^{-1}B'\hat{u}'(s) \quad (5.57)$$

$$\hat{y}(s) = C\hat{x}(s) + F'\hat{u}'(s) \quad (5.58)$$

Therefore from 5.57 and 5.58, we can have three transfer functions that provide control to input transfer function, output impedance and audio susceptibility**.**

5.3.2 MODEL OF THE BOOST CONVERTER

The state space description of the boost converter model is derived when transistor operates in on state and when it is in on state.

During the on state, transistor voltage goes zero and diode is not conducting. The circuit in figure 5.3 below is the operation during time t_{on} and current source is also added within.

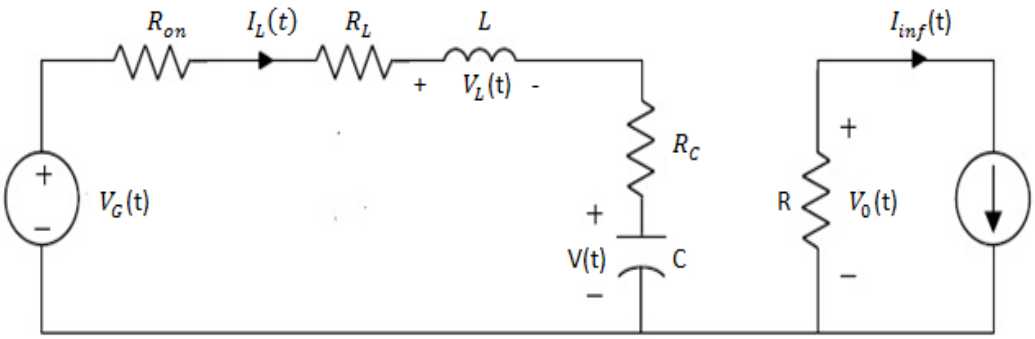

Figure 5.3 Circuit of boost operation during t_{off}

From the figure, following equations are obtained:

$$V_G(t) - L\frac{dI}{dt} - I_{inj}(t)R_L = 0 \tag{5.59}$$

$$\frac{dI_L}{dt} = \left(\frac{V_G(t) - I(t)R_L}{L}\right) \tag{5.60}$$

$$C\frac{dV(t)}{dt} = \left(-\frac{V_O(t)}{R} - I_{inj}(t)\right) \tag{5.61}$$

$$(t)\left(1 + \frac{R_C}{R}\right) = V(t) - R_C I_{inj}(t) \tag{5.62}$$

$$V_O(t) = \frac{R}{R+R_C}V(t) - \frac{RR_C}{R+R_C}I_{inj}(t) \tag{5.63}$$

$$\frac{dI(t)}{dt} = (-A_1)I(t) + V_G(t) \tag{5.64}$$

Using 5.52 and 5.53,we obtain

$$\frac{dV(t)}{dt} = \frac{1}{(R+R_C)}V(t) - \frac{R}{(R+R_C)}I_{inj}(t) \tag{5.65}$$

Therefore,

$$d\begin{bmatrix} I(t) \\ V(t) \end{bmatrix} = \begin{bmatrix} \frac{-R_L+R_{on}}{L} & 0 \\ 0 & \frac{-1}{(R+R_C)} \end{bmatrix}\begin{bmatrix} I(t) \\ V(t) \end{bmatrix} + \begin{bmatrix} \frac{1}{L} & 0 \\ 0 & \frac{-R}{(R+R_C)} \end{bmatrix}\begin{bmatrix} V_G(t) \\ I_{inj}(t) \end{bmatrix} \tag{5.66}$$

$$y(t) = \begin{bmatrix} 0 & \frac{R}{R+R_C} \end{bmatrix}\begin{bmatrix} I(t) \\ V(t) \end{bmatrix} + \begin{bmatrix} 0 & \frac{-RR_C}{(R+R_C)} \end{bmatrix}\begin{bmatrix} V_G(t) \\ I_{inj}(t) \end{bmatrix} \tag{5.67}$$

where,

$$A_1 = \begin{bmatrix} \frac{-R_L+R_{on}}{L} & 0 \\ 0 & \frac{-1}{(R+R_C)C} \end{bmatrix} \tag{5.68}$$

$$B_1 = \begin{bmatrix} \frac{1}{L} & 0 \\ 0 & \frac{-R}{(R+R_C)C} \end{bmatrix} \tag{5.69}$$

$$C_1 = \begin{bmatrix} 0 & \frac{R}{(R+R_C)} \end{bmatrix} \tag{5.70}$$

$$F_1 = \begin{bmatrix} 0 & \frac{-RR_C}{(R+R_C)} \end{bmatrix} \tag{5.71}$$

When transistor is off, using circuit in figure 5.1

$$A_2 = \begin{bmatrix} -\frac{R_L+R_{on}}{L} - \frac{RR_C}{(R+R_C)L} & -\frac{R}{(R+R_C)L} \\ \frac{R}{(R+R_C)C} & -\frac{1}{(R+R_C)C} \end{bmatrix} \tag{5.72}$$

$$B_2 = \begin{bmatrix} \frac{1}{L} & \frac{RR_C}{(R+R_C)L} \\ 0 & \frac{-R}{(R+R_C)C} \end{bmatrix} \tag{5.73}$$

$$C_2 = \begin{bmatrix} \frac{RR_C}{R+R_C} & \frac{R}{R+R_C} \end{bmatrix} \tag{5.74}$$

$$F_2 = \begin{bmatrix} 0 & -\frac{RR_C}{R+R_C} \end{bmatrix} \tag{5.75}$$

Applying state space averaging, we get

$$A = \begin{bmatrix} \frac{-D'RR_C}{(R+R_C)} - \frac{R_L+R_{on}}{L} & \frac{-D'R}{(R+R_C)L} \\ \frac{D'R}{(R+R_C)C} & \frac{-1}{(R+R_C)C} \end{bmatrix} \quad (5.76)$$

$$B = \begin{bmatrix} \frac{D}{L} & \frac{R}{(R+R_C)L} \\ 0 & \frac{-R}{(R+R_C)C} \end{bmatrix} \quad (5.77)$$

$$C = \begin{bmatrix} \frac{D'RR_C}{(R+R_C)} & \frac{R}{(R+R_C)} \end{bmatrix} \quad (5.78)$$

$$F = \begin{bmatrix} 0 & \frac{-RR_C}{(R+R_C)} \end{bmatrix} \quad (5.79)$$

The dc voltage is zero across capacitor ESR. Value of the mean current is equals the mean value of diode current. Inductor current equals to diode current during D' of the time and otherwise equals to zero.The dc amplification of boost converter is more than one.

And therefore,

$$B_d = \begin{bmatrix} \frac{V_G}{LD'} \\ \frac{-V_G}{(RD'+R_C)CD'} \end{bmatrix} \quad (5.80)$$

$$F_d = \frac{-R_C V_G}{(RD'+R_C)D'} \quad (5.81)$$

$$B' = \begin{bmatrix} \frac{D}{L} & \frac{R}{(R+R_C)L} & \frac{V_G}{LD'} \\ 0 & \frac{-R}{(R+R_C)C} & \frac{-V_G}{(RD'+R_C)CD'} \end{bmatrix} \quad (5.82)$$

$$F' = \begin{bmatrix} 0 & \frac{-RR_C}{(R+R_C)} & \frac{-R_C V_G}{(RD'+R_C)D'} \end{bmatrix} \quad (5.83)$$

Extraction of transfer functions from state space averaging:

Using 5.55, 5.56, 5.82, 5.83 in equations

$$s\hat{x}(s) = A\hat{x}(s) + B'\hat{u}'(s) \quad (5.84)$$

$$\hat{y}(s) = C\hat{x}(s) + F'\hat{u}'(s) \quad (5.85)$$

$$\hat{x}(s) = (sI - A)^{-1}B'\hat{u}'(s) \quad (5.86)$$

$$\hat{y}(s) = C\hat{x}(s) + F'\hat{u}'(s) \quad (5.87)$$

Therefore from 5.86 and 5.87, we can have three transfer functions that provide control to input transfer function, output impedance and audio susceptibility**.**

5.4 CASE STUDY:

The designed dc–dc converter when operate with following parameter are analysed. Bode plot of the transfer functions and the poles location check the stability of the transfer functions in both modes of operations.

$R_L = 45.1$

$L = .000355$

$R_C = .45$

$D = .55$

$C = 1.388 * 10^5$

$V_{IN} = V_G = 450V$

$V_O = 300V$

5.4.1 BUCK OPERATION

During buck operation, when the input voltage is 450V and voltage at the output needs to be around 300V. State space averaging model is being developed to obtain control to input transfer function, output impedance and audio susceptibility. The transfer functions are being analysed using bode plot and their corresponding poles location determined.

5.4.1.1 Z_{11}= CONTROL TO INPUT TRANSFER FUNCTION

Transfer function:$Z_{11} = \frac{518.5s+9.902e005}{s^2+1.535e005s+4.588e009}$

Bode plot:

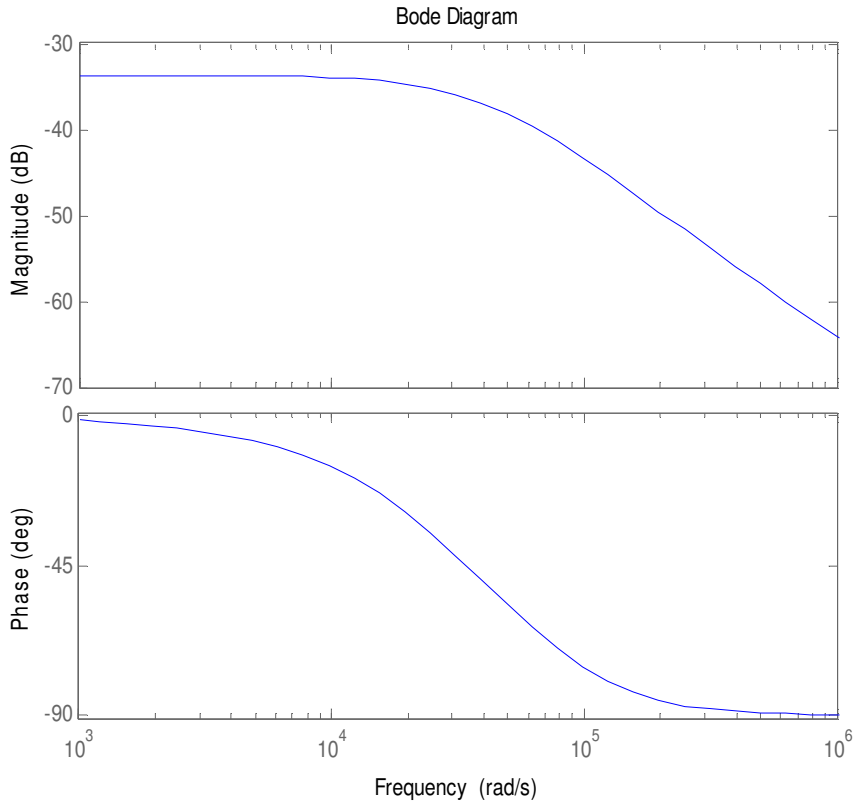

Figure 5.4 Bode plot of Control to input transfer function Z_{11}

It is found from the bode plot that the system Z_{11} is stable and is verified by poles location as well.

5.4.1.2 Z_{12}= OUTPUT IMPEDANCE

Transfer function:

$$Z_{12} = \frac{-0.3453s^2 + 1.949e004s + 9.051e009}{s^2 + 1.535e005s + 4.588e009}$$

Bode plot:

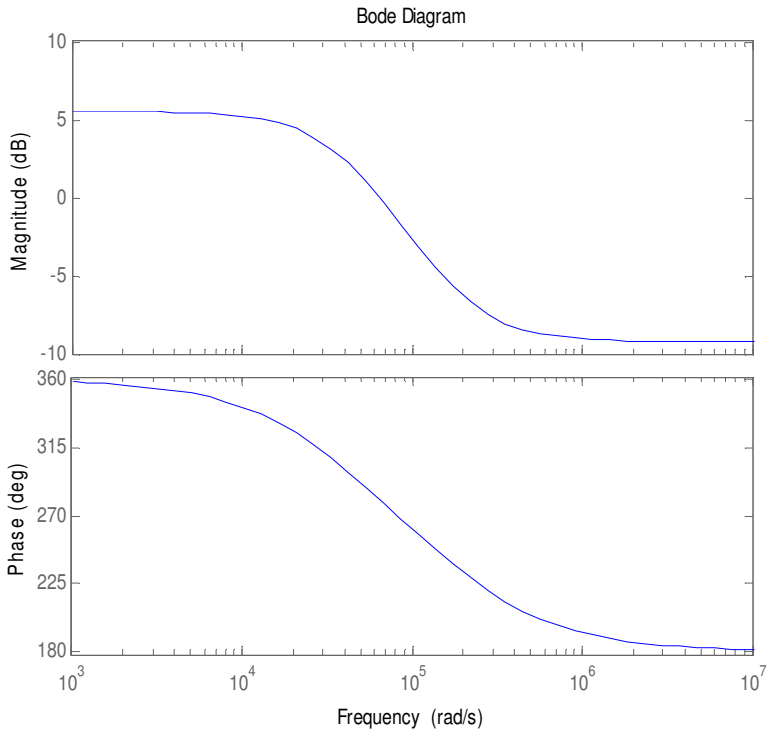

Figure 5.5 Bode plot of output impedanceZ_{12}

It is found from the bode plot that the system Z_{12} is stable and it is verified by poles location.

5.4.1.3 Z_{13}= AUDIO SUSCEPTIBILITY

Transfer function:

$$Z_{13} = \frac{4.154e005s + 5.55e010}{s^2 + 1.535e005s + 4.588e009}$$

Bode plot:

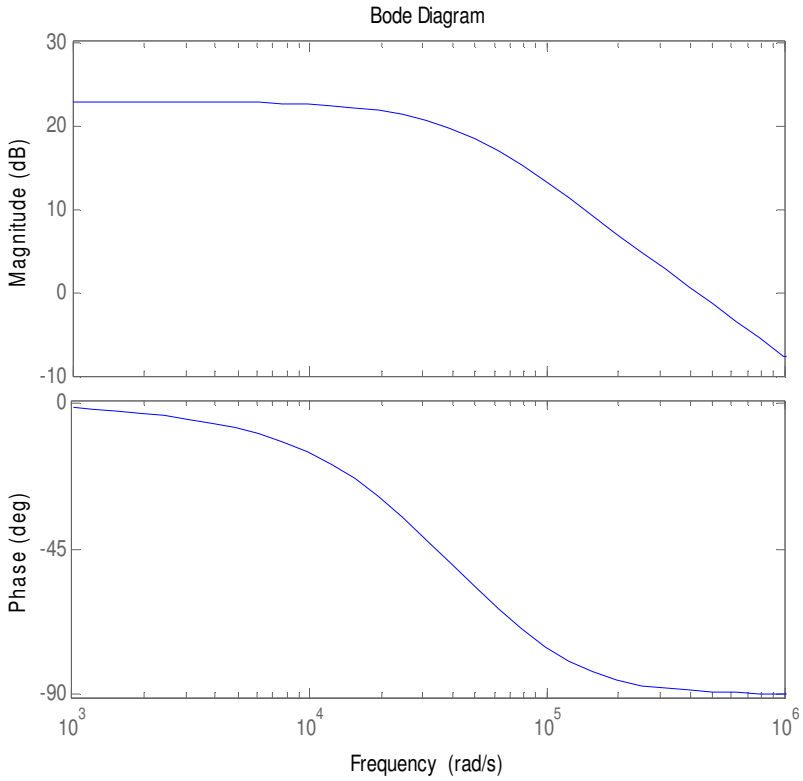

Figure 5.6 Bode plot for audio susceptibilityZ_{13}

It is found from the bode plot that the system Z_{13} is stable and is verified by poles location as well.

5.4.2 BOOST OPERATION

During boost operation we have input voltage of 300V and correspondingly there is an output voltage of 450V.It may also be interpreted as reverse buck operation**.** State space averaging model is being developed to obtain control to input transfer function, output impedance and audio susceptibility. The transfer functions are being analysed using bode plot and poles location.

5.4.2.1 Z_{21}=CONTROL TO INPUT TRANSFER FUNCTION

Transfer function:

$$Z_{21} = \frac{351.2s + 3.152e005}{s^2 + 1.255e005s + 1.403e008}$$

Bode plot:

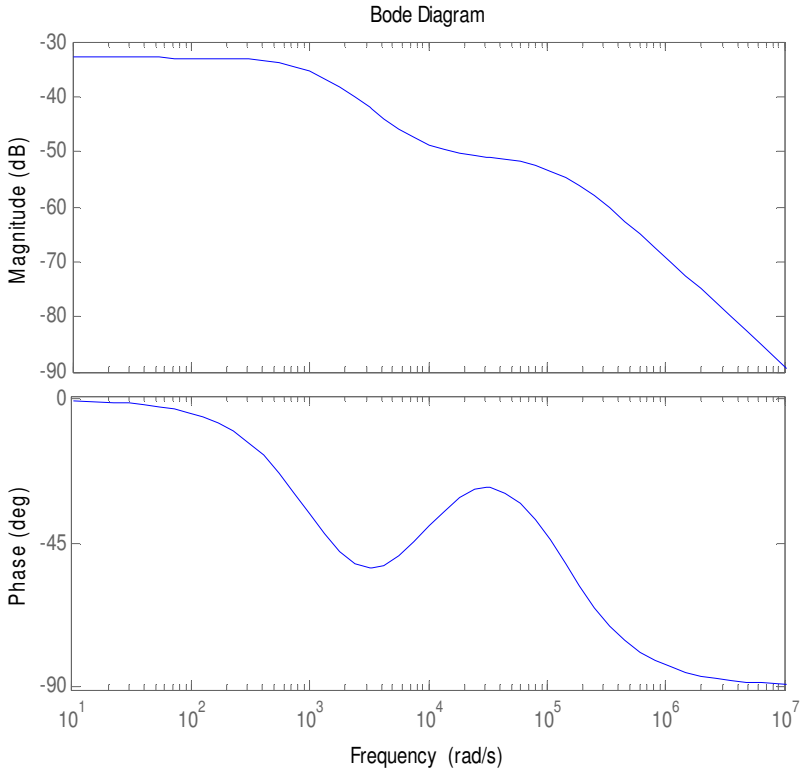

Figure 5.7 Bode plot for control to input transfer function Z_{21}

It is found from the bode plot that the system $Z_{21}$is stable and is verified by poles location as well.

5.4.2.2 Z_{22} = OUTPUT IMPEDANCE

Transfer function:

$$Z_{22} = \frac{-0.3951s^2 - 5.35e004s - 4.518e008}{s^2 + 1.255e005s + 1.403e008}$$

Bode plot:

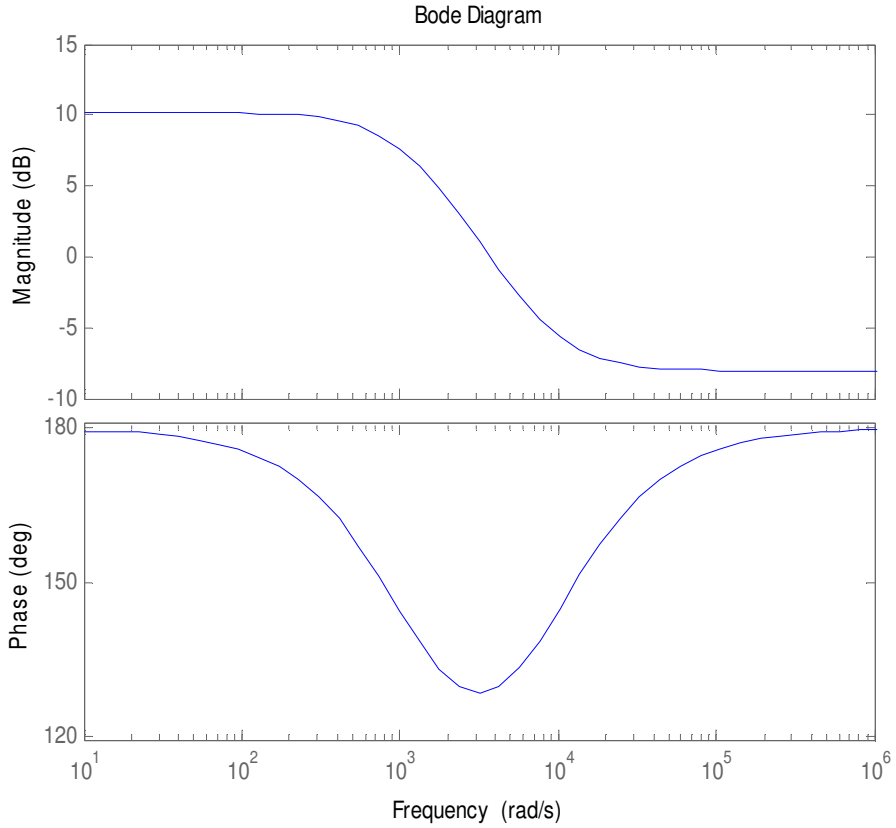

Figure 5.8 Bode plot for output impedance Z_{22}

It is found from the bode plot that the system $Z_{22}$is unstable despite negative real part of the poles.

5.4.2.3 Z_{23}=AUDIO SUSCEPTIBILITY

Transfer function:

$$Z_{23} = \frac{-54.32s^2 - 1.009e005s - 8.5404e010}{s^2 + 1.255e005s + 1.403e008}$$

Bode plot:

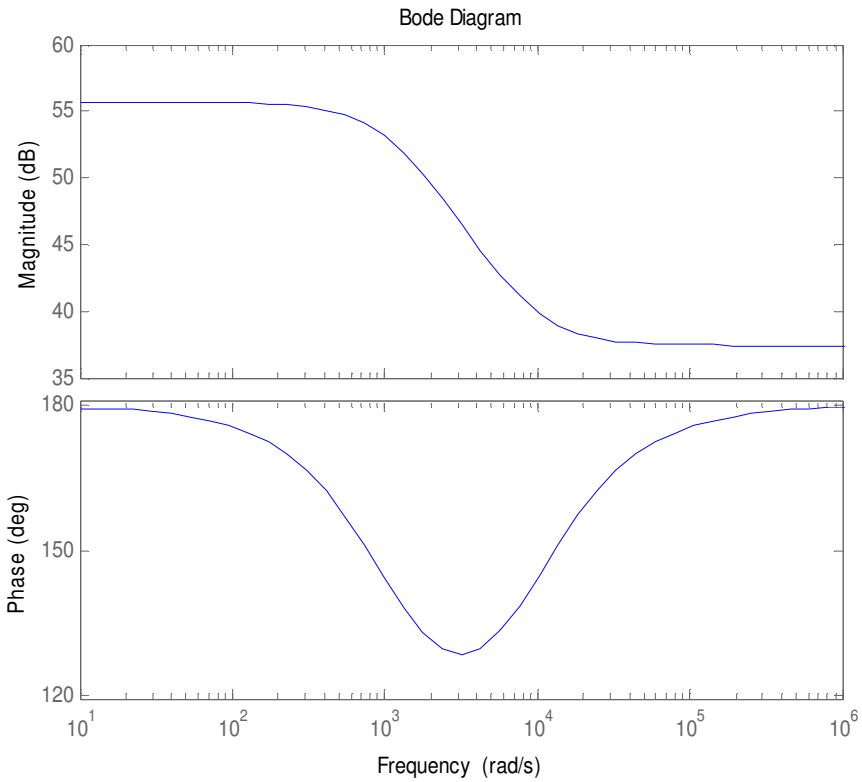

Figure 5.9 Bode plot for audio susceptibility Z_{23}

It is found from the bode plot that the system $Z_{32}$is stable and is verified by poles location as well.

5.5 CONCLUSION

State-space averaging of a non-ideal boost and buck converter has been presented. There described a DC equivalent and small-signal equivalent circuit models. Resulting small signal analysis can be analysed using Laplace transform, to know about the behaviour and properties of the converters.

Small signal analysis makes it simple to determine: (1) the line-to-output transfer function, which describes how variations or disturbances in the applied voltage lead to disturbances in the output voltage (2) the control-to-output transfer function, which describes how control

input variations influence the output voltage. (3) The input impedance, which plays a significant role when an electromagnetic interference (EMI) filter is added at the converter power input. The output impedance describes how variations in the load current affect the output voltage, etc.

CHAPTER 6

CONCLUSION AND FUTURE CONSIDERATIONS

6.1 CONCLUSION

In this dissertation, overview of the Hybrid Electric Vehicle (EHV) and bidirectional operation of dc-dc converter is discussed. Further design and analysis of dc-dc converter dedicated for Hybrid Electric Vehicle (EHV) has been presented. Analysis of the converter is done using state space averaging technique. The transfer functions are obtained for both buck as well as in boost mode of operation.

Design of the power converter is being done using pre defined methodology in which parameters are chosen to design best possible converter design. Design of the converter involved the calculation of semiconductor losses and inductor loss followed by efficiency calculation. Inductor core materials used are ferrite and iron powder material with core shapes such as EC-70 and ETD-49.The list of four combinations of type of inductor are studied and efficiencies of the power converter with these inductors are calculated.

Analysis of the power converter is carried out employing state space averaging. State space averaging is done to obtain linear time invariant system for both buck and boost modes of operation. Parameters of the designed converter are taken into consideration for state space averaging and transfer function such as control to input transfer function, audio susceptibility and output impedance are derived. Further, the bode diagrams of the transfer functions are plotted and the corresponding pole locations are determined. Result shows that all the transfer functions are stable except the output impedance for boost operation. Thus stability of all the three transfer functions for both modes of operation are being checked and analysed.

6.2 FUTURE WORK

The future scope of the proposed work is as follows:

- The power converter can be designed using other types of inductor core and a comparative analysis can be carried out with the existing design developed.
- The frequency domain parameters can be improved further for transfer functions obtained from state space averaging.
- The instability of the output impedance in boost mode of operation can be resolved using suitable compensation techniques.

REFERENCES

[1] M. Ehsani, Y. Gao, S. Gay, and A. Amade, “Modern Electric, Hybrid Electric, and Fuel Cell Vehicles: Fundamentals, Theory, and Design”, *CRCPress,* Nov 2004.

[2] Peng, M.C., F.Z., Kelly, K.J., O'Keefe, M. and Hassani, V., “Topology, Design, analysis and thermal management of power electronics for hybrid electric vehicle applications,” *International Journal on Electric and Hybrid Vehicles*, Vol. 1, No. 3, pp.276-294, 2008.

[3] Rim, C.T., Joung , G.B., Cho, G.H.,"A state-space modelling of non-ideal DC-DC converters," *19th Annual IEEE Power Electronics Specialists Conference”,* Vol.2, No.1, pp.943-950, 1988.

[4] Moussa, W.M. and Morris, J.E., "Comparison between state space averaging and PWM switch for switch mode power supply analysis, "*Proceedings of the IEEE Southern Tier Technical Conference”,* pp.15-21, 1990.

[5] Mahdavi, J., Emaadi, A., Bellar, M.D. and Ehsani, M., "Analysis of power electronic converters using the generalized state-space averaging approach," *IEEE Transactions on Circuits and Systems I: Fundamental Theory and Applications*, Vol.44, No.8, pp.767-770, Aug 1997

[6] Schupbach, R.M. and Balda, J.C., "Comparing DC-DC converters for power management in hybrid electric vehicles," *IEEE International Electric Machines and Drives Conference,* Vol.3,pp. 1369-1374,2003.

[7] Yalamanchili, K.P. and Ferdowsi, M., "Review of multiple input DC-DC converters for electric and hybrid vehicles," *IEEE Conference on Vehicle Power and Propulsion,* pp. 160- 163, 2005.

[8] Davoudi, A., Jatskevich, J. and De Rybel, T., "Numerical state-space average value modelling of PWM DC-DC converters operating in DCM and CCM," *IEEE Transactions on Power Electronics,* Vol.21, no.4, pp.1003-1012, 2006.

[9] Jih-Sheng Lai, Nelson, D.J., "Energy Management Power Converters in Hybrid Electric and Fuel Cell Vehicles," *Proceedings of the IEEE*, Vol.95, no.4, pp.766-777, 2007.

[10] Bellur, D.M., Kazimierczuk, M.K., "DC-DC converters for electric vehicle applications," *Electrical Insulation Conference and Electrical Manufacturing Expo,* pp.286-293, 2007.

[11] Silvestre, J., "Half-bridge bidirectional DC-DC Converter for small Electric Vehicle," *International Symposium on Power Electronics, Electrical Drives, Automation and Motion,* pp. 884-888, 2008.

[12] Nwosu, C.A., "State-Space Averaged Modelling of a Nonideal Boost Converter". *Pacific Journal of Science and Technology*. Vol.9, no.2,pp.302-308, 2008.

[13] Du, Y., Zhou, X., Bai, S., Lukic, S., and Huang, A, "Review of non-isolated bi-directional DC-DC converters for plug-in hybrid electric vehicle charge stationapplication at municipal parking decks," *Twenty-Fifth Annual IEEE Conference and Exposition on Applied Power Electronics*, pp.1145-1151, 21-25, 2010.

[14] Ahmadi, M., Shenai, K., "New, efficient, low-stress buck/boost bidirectional DC- DC converter, "*Energy Tech,* pp.1-6, 29-31, 2012.

[15] Sihun Yang; Goto, K., Imamura, Y., Shoyama, M., "Dynamic characteristics model of bi-directional DC-DC converter using state-space averaging method," *34th International Conference on Telecommunications Energy,* pp.1-5, 2012.

[16] Zahedi, B., Nebb and O.C., Norum., L.E.," An isolated bidirectional converter modelling for hybrid electric ship simulations," *Transportation Electrification Conference and Expo (ITEC),* pp.1-6, 2012.

[17] Kumar, L. and Jain, S, "A multiple input dc-dc converter for interfacing of battery/ultracapacitor in EVs/HEVs/FCVs," *IEEE 5th International Conference on Power Electronics (IICPE),* pp.1-6, 2012.

[18] Mohan, N., Undeland, Robbins, “Power Electronics Converters, applications and design”, *John Wiley & sons*, 3rd Edition , Inc., pp. 760-767,2003.

[19] Erickson, R.W., “Fundamentals of Power Electronics”, Nowell, MA: *Kluwer Academic Publishers*, 2nd. Edition, 2001.

[20] Edition 2009-01-29, Published by Infineon Technologies AG, Am Campeon 1-12, 85579 Neubiberg, Germany, Infineon Technologies AG 2006.

[21] http://www.ferroxcube.com/prod/assets/ec70.pdf

[22] http://www.ferroxcube.com/prod/assets/etd49.pdf

[23] http://igbt.cn/admin/productfile/BSM300GB60DLC.pdf

[24] Thaler, G.J., “Automatic Control System” *West Publishing Company*: St. Paul, MN.,1989

[25] Fargeon, C.,“The Digital Control of Systems” *Van No strand Reinhold*: New York, NY, 1989.

PUBLICATIONS

Work carried out in this dissertation resulted in the following publications:

Papers submitted-

[1] Dharam Dutta and Souvik Ganguli , "Design of a Bidirectional DC-DC Converter for Hybrid Electric Vehicles (HEV) Using MATLAB", *International Journal of Advanced research in Electrical, Electronics and Instrumentation Engineering.(Under review*)

[2] Dharam Dutta and Souvik Ganguli ,"Design Aspects of Bidirectional DC-DC converter for Hybrid Electric Vehicles: A Brief Review and Future Directions", *Journal of the Institute of Engineering,* Tribhuvan University, Nepal *(Under review)*

[3] Dharam Dutta and Souvik Ganguli ,"State Space Average Modelling of DC-DC Converter for Hybrid Electric Vehicles"*, International Journal of Electric and Hybrid Vehicles,* Inderscience Publishers.*(To be communicated)*